



HAL
open science

Frequency derivative of Rayleigh wave phase velocity for fundamental mode dispersion inversion: parametric study and experimental application

Ao Wang, Donatienne Leparoux, Odile Abraham, Mathieu Le Feuvre

► To cite this version:

Ao Wang, Donatienne Leparoux, Odile Abraham, Mathieu Le Feuvre. Frequency derivative of Rayleigh wave phase velocity for fundamental mode dispersion inversion: parametric study and experimental application. *Geophysical Journal International*, 2021, 224 (1), pp. 649-668. 10.1093/gji/ggaa417. hal-03081526

HAL Id: hal-03081526

<https://hal.science/hal-03081526>

Submitted on 18 Dec 2020

HAL is a multi-disciplinary open access archive for the deposit and dissemination of scientific research documents, whether they are published or not. The documents may come from teaching and research institutions in France or abroad, or from public or private research centers.

L'archive ouverte pluridisciplinaire **HAL**, est destinée au dépôt et à la diffusion de documents scientifiques de niveau recherche, publiés ou non, émanant des établissements d'enseignement et de recherche français ou étrangers, des laboratoires publics ou privés.

Frequency derivative of Rayleigh wave phase velocity for fundamental mode dispersion inversion: parametric study and experimental application

A. Wang, D. Leparoux, O. Abraham and M. Le Feuvre

GERS-GeoEND, Univ Gustave Eiffel, Campus Nantes, IFSTAR, Allée des Ponts et Chaussées, Routes de Bouaye - CS 5004, 44344 Bouguenais, France.
E-mail: ao.wang@univ-eiffel.fr, donatienne.leparoux@univ-eiffel.fr, odile.abraham@univ-eiffel.fr

Accepted 2020 September 3. Received 2020 August 7; in original form 2019 September 26

SUMMARY

Monitoring the small variations of a medium is increasingly important in subsurface geophysics due to climate change. Classical seismic surface wave dispersion methods are limited to quantitative estimations of these small variations when the variation ratio is smaller than 10 per cent, especially in the case of variations in deep media. Based on these findings, we propose to study the contributions of the Rayleigh wave phase velocity derivative with respect to frequency. More precisely, in the first step of assessing its feasibility, we analyse the effects of the phase velocity derivative on the inversion of the fundamental mode in the simple case of a two-layer model. The behaviour of the phase velocity derivative is first analysed qualitatively: the dispersion curves of phase velocity, group velocity and the phase velocity derivative are calculated theoretically for several series of media with small variations. It is shown that the phase velocity derivatives are more sensitive to variations of a medium. The sensitivity curves are then calculated for the phase velocity, the group velocity and the phase velocity derivative to perform quantitative analyses. Compared to the phase and group velocities, the phase velocity derivative is sensitive to variations of the shallow layer and the deep layer shear wave velocity in the same wavelength (frequency) range. Numerical data are used and processed to obtain dispersion curves to test the feasibility of the phase velocity derivative in the inversion. The inversion results of the phase velocity derivative are compared with those of phase and group velocities and show improved estimations for small variations (variation ratio less than 5 per cent) of deep layer shear wave velocities. The study is focused on laboratory experiments using two reduced-scale resin-epoxy models. The differences of these two-layer models are in the deep layer in which the variation ratio is estimated as 16.4 ± 1.1 per cent for the phase velocity inversion and 17.1 ± 0.3 per cent for the phase velocity derivative. The latter is closer to the reference value 17 per cent, with a smaller error.

Key words: Inverse theory; Time-series analysis; Acoustic properties; Surface waves and free oscillations.

1 INTRODUCTION

The subsurface media are particularly affected by climate change and associated climatic events through variations in water table levels and fluid transfers in the unsaturated zone, known as the Critical Zone. These phenomena create alteration zones that can potentially lead to collapses. For these reasons, monitoring mechanical changes in the subsurface media in areas of human activity, particularly when they involve buildings, is becoming increasingly important. These needs are therefore among the key issues of current geophysical research.

Among non-destructive seismic approaches for assessing the mechanical properties of shallow underground media, the properties of surface waves are widely used due to the energy they transport and their long propagation distances (Socco & Strobbia 2004; Foti *et al.* 2018). Using the dispersion of surface waves in a layered structure, the properties of the medium are inferred by solving an inverse problem. This method, as a standard procedure for surface wave analysis, contains three steps: (1) acquisition, (2) processing for extracting the dispersion data that will serve as the inversion input data and (3) the inversion whose output parameters are shear wave velocity, compressional-wave velocity and density, as

function of depth. Classically the phase velocity dispersion is used for subsurface investigations, and the group velocity dispersion is used for seismology approaches. The common methods to extract these two dispersion data are recalled below.

A sensitivity study by Bhattacharya (2015) showed that group velocity is more efficient than phase velocity to explore the anisotropic nature of a medium. The multiple filter method (MFM) proposed by Dziewonski *et al.* (1969) is based on bandpass frequency filters to analyse earthquake signals. Using different bandpass filters, waves with frequencies around the centre frequency are isolated. Thus, the delay between the source wavelet and the arrival of the signal, both filtered for the current frequency, is used for assessing the group velocity corresponding to the current frequency. The main difficulty in using the multiple filter technique is the possible interference between higher modes when the envelope of the filtered signals is not sharp enough to contain a very narrow frequency band (Gabriels *et al.* 1987). Based on MFM, the reassignment method (Kodera *et al.* 1976; Auger & Flandrin 1995) calculates the centre of gravity of a signal pulse, which helps improve the accuracy of the group velocity assessment. Pedersen *et al.* (2003) developed a good adaptation for both synthetic seismograms and field data relating to shallow earth structures. However, the reassignment can blur the distinction between waves that are located close together, thus generating complexity in the time–frequency domain. In addition, in the case of strong frequency dispersion, the phase velocity can be efficiently extracted for several modes if a large set of receivers is involved (Socco & Strobbia 2004). Thus, as mentioned by these authors, this dispersion data, that is, the phase velocity, is commonly used in subsurface investigation. The principal of its extraction is explained below.

Indeed, the classical measurement set-up for subsurface geophysics applications involves a set of several receivers for a processing method called MASW (multichannel analysis of surface waves). This approach, first implemented by geophysicists in the 1980s for near-surface characterization (McMechan & Yedlin 1981; Gabriels *et al.* 1987) and improved in the following decades (Park *et al.* 1998; Foti *et al.* 2000), is the most commonly used method in the case of geophysical Near Surface investigations. By applying an active source and a linear array of receivers, the MASW method enhances the production rate in the field and makes the processing of the data faster, less subjective, and more robust compared to classical one-source one-receiver systems (Foti *et al.* 2014). The processing stage consists in extracting from recordings the dispersion data that will be inverted. With the MASW approach, the dispersion data comprises the dispersion curves of the phase velocity. Several signal processing techniques can be used for extracting it, such as the $f-k$ transform (Yilmaz 2001), the $\tau-p$ transform (McMechan & Yedlin 1981), the phase-difference method (Mokhtar *et al.* 1988; Park *et al.* 1998), or the linear Radon transform (Luo *et al.* 2008). The phase-difference method, achieved by processing an optimization of the $\tau-p$ transform, provides a high spectrum resolution of the dispersion diagram with an optimized number of receivers (Park *et al.* 1998; Socco *et al.* 2010; Xia 2014). It has been chosen for this study. For this procedure, the Fourier Transform is applied to each signal of the seismic shot. After normalizing the amplitude, a phase shift correction is applied to each frequency component as a function of the receiver-source distance, through a series of possible phase velocities. The corrected frequency components are summed over the entire shot to obtain a dispersion diagram in the $v-f$ domain. On the latter, the areas of maximum values correspond to the extracted phase velocity estimated as a function of frequency for the fundamental mode and the excited higher modes.

Whatever the dispersion data used (i.e. group or phase velocity), the general approach of dispersion inversion of surface waves makes it possible to characterize the propagating media for investigating the Earth on a global scale up to the first metre deep or even the sub-millimetre scale, depending on the propagating wavelength range used. Thus, surface wave analysis should be suitable for monitoring the mechanical variations of the subsurface. For example, Planès *et al.* (2016) used the passive seismic-interferometry technique to analyse internal erosion in earth dams and levees. They were able to monitor a 20 per cent reduction in surface wave velocity on a canal embankment model and a 30 per cent variation in a field-scale levee testing experiment. The same technique has been used on a sea levee in the Netherlands, using traffic noise on a bridge and the noise from a wind turbine as sources, and a 3–5 per cent increment of the group velocity was estimated during low tide (Planès *et al.* 2017). Joubert *et al.* (2018) applied the cross-correlation and deconvolution methods of seismic noise, to estimate a variation of less than 10 per cent of relative surface wave velocity as a function of increasing sea level. It is noteworthy that these authors did not apply any inversion processing to their data sets.

Indeed, in the case of slight modifications in the medium, the inversion method must discriminate small parameter variations leading to several issues that alter the efficiency of the process and degrade its potential. These inaccuracies are due to accuracy limits in acquisition, dispersion data extraction, or inversion processes. Note that using passive measurements makes possible to continuously record the signal without any action at the source from the geophysicist. The problem of measurement errors is different from the active set-up, but the inversion process is similar with the same limit problems. To overcome the problem of acquisition and phase velocity extraction, different works have proposed new approaches as a function of field conditions. For example, Le Feuvre *et al.* (2015) improved the determination of subsurface shear wave velocity from ambient noise using cross-correlations and beamforming. Dangeard *et al.* (2018) proposed a statistical approach for estimating picking errors in the case of standard surface wave inversion for time-lapse studies. The latter tackled the repeatability issue of the method but did not overcome the Realistic Error, the term given by O'Neill (2004), who used a statistical approach to define an uncertainty law for the extraction of the phase velocity. Studies on these effects (O'Neill 2004; Lai *et al.* 2005) proved that the uncertainty in surface wave measurements has a greater impact on low frequencies, making it more difficult to assess deep media variations precisely. More recently, studies in a two-layer medium (Wang *et al.* 2018) showed that conventional phase velocity dispersion curve inversion is not capable of estimating a variation ratio lower than 10 per cent in the deep layer. Other possibilities for increasing the efficiency of results could be used to tackle the inversion process, for example the misfit function, which can be based on different norms or diagram distances (e.g. Wang *et al.* 2019).

We can summarize the needs and problems described above as follows. The publications on dike monitoring mentioned show the interest of surface waves to identify areas of damage and water penetration. In order to monitor detailed evolutions before a potential break, the methodology must allow identifying small variations in surface wave velocity. This is not straightforward or even possible for the inversion of surface wave dispersion in the current classical procedure. In order to improve its performances, different levers can be used, some of which have been analysed in the literature, such as errors on measurements and dispersion data extraction, or the distance norm between estimated and recorded data. However, despite the progress made in these studies, the results available are

not sufficient to make the methodology effective if phase velocity variations are lower than 20 per cent. Therefore, we propose here to study another lever that is complementary to the previous ones.

In this framework, our concern is to study the effect of the Rayleigh phase velocity derivative with respect to frequency dV_{ph}/df (abbreviated as PVD). More particularly, our aim is to study its sensitivity and impact on the convergence and precision of the inversion results. This proposition is based on the idea that information on the variation of a medium's properties as a function of depth is contained in the variation of the phase velocity as a function of frequency and thus potentially in the phase velocity derivative. Consequently, the PVD could provide more sensitive information on the shear wave velocity depth profile in the medium. First, to analyse the sensitivity of the PVD, qualitative and quantitative approaches regarding its behaviour will be implemented before testing it on the inversion process. For these analyses, all the stages of the methods (including the geometry of the measurement set-up and the inversion process) follow the most usual procedures for geophysical approaches in shallow media. The inversion method used is summarized hereafter.

The inversion stage consists in assessing the shear wave velocity 1-D model from surface wave dispersion data. To do this, a local or a global optimization method can be used. The global approach, which is used for our study, makes it possible to explore the parameter space without defining any initial model. It provides a set of possible models associated with a value of the misfit function. The latter indicates the error level, for example, thanks to an L2 norm, between the dispersion data extracted from measurements and those theoretically calculated. More precisely, the global optimization method used for this study is based on the neighbourhood algorithm (NA), commonly used by geophysicists. The NA is a stochastic search method in a given parameter space, making use of Voronoi cells to compute the misfit function in the parameter space (Sambridge 1999). Like other global inversion methods (genetic algorithm, simulated annealing, etc.), the NA generates pseudo-random samples in the parameter. The originality of NA is that the new samples generated at each iteration are guided and improved by the previous ones. A later study by Wathelet (2008) improved the capacity of random model generation in a parameter space with irregular boundaries.

All these process stages will be used here for a two-layer medium with increasing shear wave and compressional-wave velocities as a function of depth, and for the fundamental mode which is considered as the most preponderant in this case (Socco *et al.* 2010; Foti *et al.* 2014). The aim is to determine the fundamental effects of the PVD on the most basic underground medium in the 1D case. The paper is organized as follows:

In a first part below, the two-layer reference model, the PVD dV_{ph}/df , and its extraction are presented. In the second part, the behaviour of the PVD is analysed qualitatively by observing its variations over a frequency range for small velocity modifications. In the next part, the theoretical sensitivity of the PVD is calculated and analysed. All these features are compared to those of the traditional dispersion data: the phase velocity and the group velocity of Rayleigh Waves. Then, inversion tests are provided and analysed in the two last parts. These tests are performed respectively on theoretical dispersion curves and on experimental data recorded in the laboratory using two-layer resin models with a shear wave velocity difference equal to 17 per cent in the deep layer. These measurement data sets are obtained to simulate at reduced scale field recordings carried out for typical shallow underground media.

2 DEFINITION AND FORMULATION OF THE PHASE VELOCITY DERIVATIVE

In a homogeneous isotropic elastic linear medium, Rayleigh wave velocity is independent of frequency. The Rayleigh phase velocity V_{ph} and group velocity V_g are equal. However, in a multilayered medium, phase and group velocities are functions of the angular frequency ω (with the relation $\omega = 2\pi f$ and f being the frequency) and wavenumber k , and defined as follows:

$$V_{ph} = \frac{\omega}{k} \quad (1)$$

$$V_g = \frac{d\omega}{dk}. \quad (2)$$

The Rayleigh phase velocity can be written as a function of frequency, wavenumber and medium parameters \mathbf{m}_j (shear wave velocity V_s , compressional-wave velocity V_p , layer thickness h and density ρ) with $j \in [1, 4]$:

$$V_{ph} = f(V_s, V_p, h, \rho, \omega, k). \quad (3)$$

Then, the phase velocity derivative can be expressed as follows:

$$dV_{ph} = \left[\frac{\partial V_{ph}}{\partial \omega} \right]_{k, m_j} d\omega + \left[\frac{\partial V_{ph}}{\partial k} \right]_{\omega, m_j} dk + \sum_i^4 \left[\frac{\partial V_{ph}}{\partial m_j} \right]_{k, \omega} dm_j. \quad (4)$$

Since the medium parameters are independent of frequency, we can write $dm_j/d\omega = 0$. Then, dividing by the term $d\omega$ on both sides of eq. (4) gives

$$\frac{dV_{ph}}{d\omega} = \left[\frac{\partial V_{ph}}{\partial \omega} \right]_{k, m_j} + \left[\frac{\partial V_{ph}}{\partial k} \right]_{\omega, m_j} \frac{dk}{d\omega}. \quad (5)$$

The partial derivatives of phase velocity with respect to frequency $[\partial V_{ph}/\partial \omega]_k = 1/k$ and to wavenumber $[\partial V_{ph}/\partial k]_\omega = -\omega/k^2$ are substituted in eq. (5):

$$\frac{dV_{ph}}{d\omega} = \frac{1}{k} - \frac{\omega}{k^2} \frac{dk}{d\omega}, \quad (6)$$

and with the definition of group velocity in eq. (2):

$$\frac{dV_{ph}}{d\omega} = \frac{1}{k} - \frac{\omega}{k^2} \frac{1}{V_g}. \quad (7)$$

Therefore, the analytical formulation of the phase velocity derivative with respect to frequency is

$$\frac{dV_{ph}}{df} = \frac{V_{ph}(V_g - V_{ph})}{fV_g}. \quad (8)$$

Eq. (8) shows that the phase velocity derivative can be formulated as a function of the group and phase velocities, according their theoretical definitions. Note that since surface waves are mostly sensitive to shear wave velocity (Takeuchi *et al.* 1972; Lai & Rix 1998; Aki & Richards 2002), only shear wave velocity variations are considered in the following study (see sensitivity formulations in Section 4). To study the PVD dV_{ph}/df , sensitivity to small variations is first analysed qualitatively and compared with the Rayleigh wave phase and group velocities. The study is based on a two-layer medium whose parameters are given in Table 1 with V_{p_i} being the compressional-wave velocity of the i th layer, V_{s_i} the shear wave velocity, ρ the density and ν_i the Poisson's ratio. The thickness of the top layer is 8 m and the deep layer is assumed to be semi-infinite.

To understand the basic behaviour of dV_{ph}/df , the study proposed here deals with a 1-D two-layer model as it is the most basic medium.

Table 1. Parameters of a two-layer reference model. V_p : compressional-wave velocity; V_s : shear wave velocity; ρ : density; ν : Poisson's ratio; h : layer thickness.

Layer (i)	$V_{p_i}^{\text{ref}}$ (m s $^{-1}$)	$V_{s_i}^{\text{ref}}$ (m s $^{-1}$)	ρ_i^{ref} (kg m $^{-3}$)	ν_i^{ref}	h_i^{ref} (m)
1	1000	600	1500	0.22	8
2	2000	1100	2200	0.28	∞

The parameter values are chosen to be typical of simple subsurface media, as an illustrative case for the qualitative analysis. However, the analysis below is based on non-dimensional observations in order to be generalizable.

3 PARAMETRIC STUDY

Based on the reference model given in Table 1, we conducted a qualitative analysis of the inversion input data V_{ph} , V_g and the PVD with respect to frequency, dV_{ph}/df , to highlight the effects of the shear wave velocity and first layer depth variations. The Geopsy software (Wathelet et al. 2004) is used to calculate the theoretical phase and group dispersion curves. The computation of the theoretical dispersion curve is based on the eigenvalue problem originally described by Thomson (1950) and Haskell (1953) and then modified by Dunkin (1965). The propagator matrix method (Gilbert & Backus 1966) is used to solve the eigenvalue problem in a 1-D stratified medium. The root search is based on the Lagrange polynomial, which efficiently speeds up the calculations. Thanks to the rapidity of the computation, a series of phase and group dispersion curves are calculated for various media following the variation ratio defined as

$$\alpha(V_{s_i}) = \frac{\Delta V_{s_i}}{V_{s_i}^{\text{ref}}} = \frac{V_{s_i}^{\text{var}} - V_{s_i}^{\text{ref}}}{V_{s_i}^{\text{ref}}} \quad (9)$$

with $V_{s_i}^{\text{ref}}$ being the reference shear wave velocity given in Table 1 and $V_{s_i}^{\text{var}}$ the variable shear wave velocity of the medium. The dispersion curves are calculated in a frequency band [1, 150] Hz and represented as a function of wavelength normalized by the interface depth h_1 in order to obtain results that can be generalized as much as possible to other similar cases (i.e. other ranges of values but similar ratios compared to the propagating wavelength).

3.1 V_{s_1} variation

The shear wave velocity of the first layer varies with a variation ratio $\alpha(V_{s_1}) \in [-5, 5]$ per cent and a corresponding Poisson's ratio $\nu_1 \in [0.17, 0.26]$. Fig. 1 shows, on the left, the phase and group velocities of the Rayleigh wave, as well as dV_{ph}/df , as a function of $\frac{\lambda}{h_1}$. The right-hand part of Fig. 1 shows variations of dispersion data (ΔV_{ph} , ΔV_g , $\Delta \partial_f V_{\text{ph}}$), normalized by the reference dispersion curves

$$(\Delta X)_{\text{norm}} = \frac{\Delta X}{X_{\text{ref}}} \times 100\% = \frac{X_{\text{var}} - X_{\text{ref}}}{X_{\text{ref}}} \times 100\% \quad (10)$$

with X being the dispersion data and X_{ref} the reference dispersion data when $\alpha(V_{s_1}) = 0$.

Fig. 1 shows that V_{ph} and V_g vary over a wider range than dV_{ph}/df for the wavelength range taken into account. However, the values of the dispersion data variations are higher when normalized by the reference model values. As expected, it can be seen that when the shear wave velocity of the first layer varies, the variations of V_{ph} are larger for short wavelengths, that is, higher frequencies. Also, for $\lambda \geq 4h_1$, they become very weak, which makes them indistinguishable

from each other. Regarding the group velocity, the variations are also larger for shorter wavelengths and the maximum is reached for $\lambda \approx 3h_1$.

dV_{ph}/df curves present variations over a different frequency range. Indeed, dV_{ph}/df tends to zero for lower wavelengths for which the Rayleigh wave penetrates only in the shallow layer. When $\lambda \approx 3.2h_1$, where the values of $\delta V_{\text{ph}}/\delta f$ are minimum, their variations are significant and reach a normalized value equal to 20 per cent for a 5 per cent variation of velocity whereas it is about 10 per cent for the group velocity. $(\Delta \partial_f V_{\text{ph}})_{\text{norm}} = 0$ at $\lambda \approx 5h_1$ and when $\lambda \geq 5h_1$, the variations are not as large as at short wavelengths. However, they are more visible than the second lobes at $(\Delta V_{\text{ph}})_{\text{norm}}$ or $(\Delta V_g)_{\text{norm}}$.

Regarding the behaviour for $\lambda = 3.2h_1$, a physical explanation can be given by analysing the cumulative amplitude of displacement in depth depending on the wavelength. The figures are presented in Appendix B. Indeed, for the wavelength $\lambda = 3.2h_1$, the normalized amplitude of the particle displacement is 0.5 at the depth corresponding to the interface between the two media and the normalized cumulative amplitude is 0.5 (see Fig. B1 in Appendix B). This means that at the wavelength $\lambda = 3.2h_1$, 50 per cent of the cumulative amplitude of the surface wave propagates in the shallow layer and 50 per cent in the deep layer. Therefore, at this point, the propagation of the Rayleigh wave is influenced by both media. The cumulative amplitude derivative with respect to wavelength confirms that the variation is highest at $\lambda = 3.2h_1$ around the interface. By varying the frequency slightly, the dominant influence comes from the shallow or deep layer, depending on the direction of the variation. This corresponds to the inflection point of the phase velocity curve, where the absolute value of the first derivative (as a function of frequency) is maximal.

3.2 V_{s_2} variation

The shear wave velocity of a semi-infinite medium varies with the variation of ratio $\alpha(V_{s_2}) \in [-5, 5]$ per cent which gives a Poisson's ratio of $\nu_2 \in [0.25, 0.31]$. Variations of phase and group velocities (V_{ph} , V_g) and the derivative of phase velocity dV_{ph}/df are shown in Fig. 2.

It can be seen that the phase velocity is sensitive to variations of the deep layer at long wavelengths and the variations become increasingly larger as the wavelength grows. The same occurs for the group velocity: $(\Delta V_g)_{\text{norm}}$ equals zero at short wavelengths and increases as the wavelength increases. The values of $(\Delta V_g)_{\text{norm}}$ is maximum when $\lambda \approx 3.4h_1$ and returns to zero at $\lambda \approx 5.3h_1$. Then, with a change of sign, the variations of the group velocity are significant at long wavelengths. Variations of V_{s_2} do not change the minima $\delta V_{\text{ph}}/\delta f$ location at $\lambda = 3.2h_1$. The variation of dV_{ph}/df is maximum and decreases gradually along the wavelength with an inflection point around $\lambda = 5.3h_1$ where $(\Delta V_g)_{\text{norm}} = 0$.

3.3 h_1 variation

The PVD is a derivative of the phase velocity as a function of frequency, and which is used to calculate the phase velocity

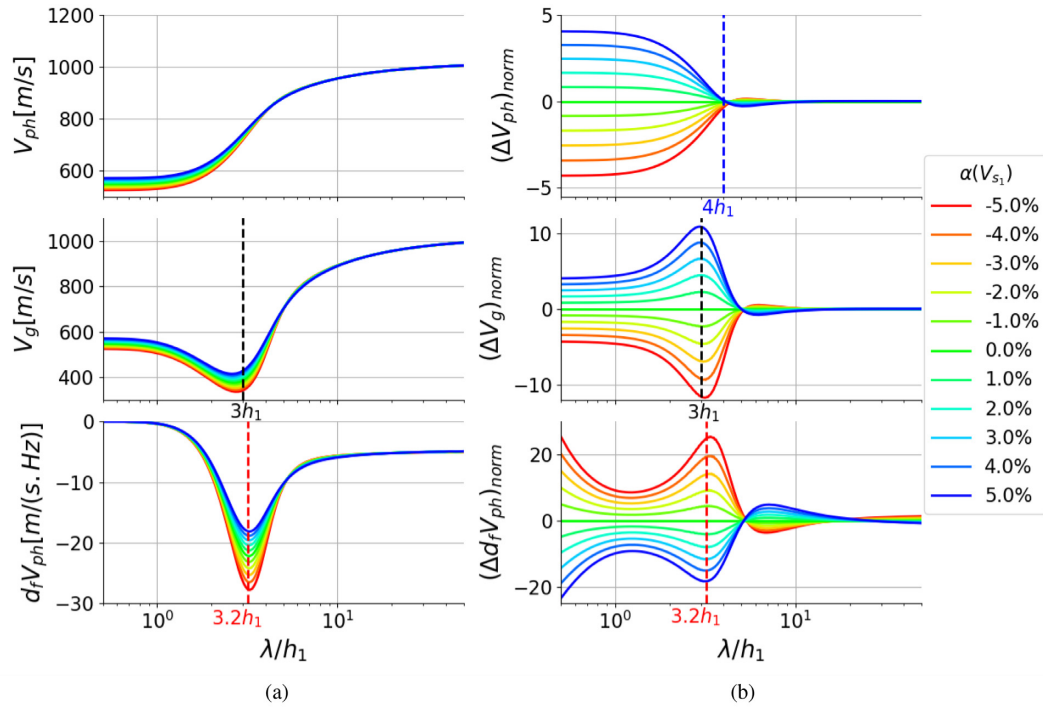


Figure 1. (a) Dispersion curves of the Rayleigh wave phase velocity (top), group velocity (middle) and phase velocity derivative (bottom) with the variation ratio $\alpha(V_{s_1}) = \pm 5$ per cent. (b) Normalized variations with respect to the dispersion curves of the reference model.

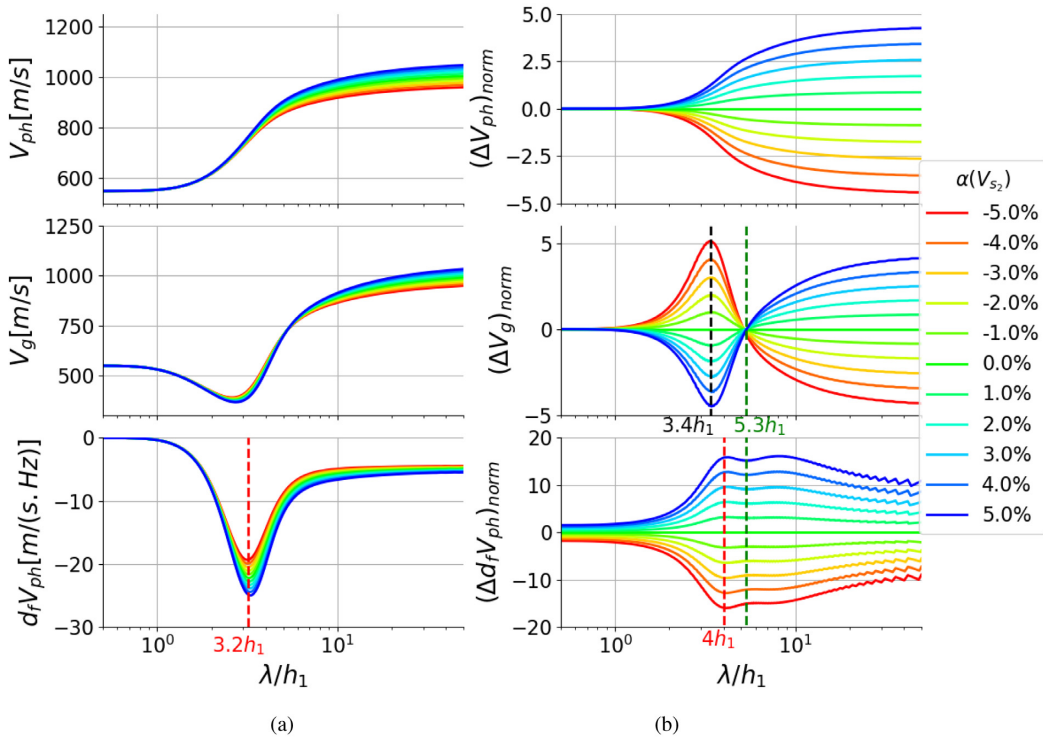


Figure 2. (a) Dispersion curves of the Rayleigh wave phase velocity (top), group velocity (middle) and phase velocity derivative (bottom) with the variation of ratio $\alpha(V_{s_2}) = \pm 5$ per cent. (b) Normalized variations with respect to reference model dispersion curves.

gradient. In a two-layer medium, the depth of the first layer changes the slope of the phase velocity dispersion curve. In the following we consider a variation in the depth of the first layer.

Interestingly, for a two-layer medium, the gradient of both the phase and group velocity dispersion curves with respect to wavelength is a linear function related to the thickness of the shallow layer, causing the minimum phase velocity derivative to occur

at $\lambda = 3.25h_1$. Normalized variations (Fig. 3) show that the group velocity is more sensitive to changes in the depth of a shallow medium than the phase velocity, while the variations of the phase velocity derivative are much larger.

It is important to note that $(\Delta\partial_r V_{ph})_{\text{norm}}$ approaches infinity at a short wavelength for $h_1 = 4$ m and 6 m. This is because when calculating the relative difference, the reference curve approaches zero at a short wavelength, but the absolute difference between the reference and variation curves is relatively large, leading to a ratio close to infinity. This reflects the instability of the PVD at high frequencies, which demands precise processing of the measurement data, since small changes of data may cause huge deviations in the inversion results, thus affecting the overall assessment of the media. This requires more attention especially for inversion, as discussed in Section 5: Inversion Tests. However, in this first stage of the study, the results indicate that the high sensitivity of the PVD could lead to more accurate assessment of the evaluation properties of the depth profile V_s . Indeed, the sensitivity of the PVD under study is high at intermediate frequencies for which the dispersion data are generally stable if the frequency range of the source is chosen correctly. This would therefore permit distinguishing small differences between two media or small variations between two states of the same medium, such as in the case of monitoring the variation of water penetration in sea dikes (Planès *et al.* 2017; Joubert *et al.* 2018), or the water content in granular material (Pasquet *et al.* 2016; Dangeard *et al.* 2018).

Before testing this numerically with the inversion process, we propose in the following part to analyse the theoretical sensitivity behaviour of the PVD. This approach will provide a general result regarding the points identified above.

4 SENSITIVITY KERNELS

The formulation of the sensitivity of the inversion input data to changes in a medium parameter is given by the partial derivative of this inversion data with respect to the medium parameter. Sensitivity can thus be calculated for the fundamental mode which is the subject of this study. It is intended to provide quantitative information on the effect of the medium variation on the inversion input data of interest, prior to future studies on the effects of higher modes, following the same principle. Here we follow the approach established by Aki & Richards (2002) for Love waves and apply it to Rayleigh waves to quantitatively compare the behaviour of the different inversion input data analysed, that is, phase velocity, group velocity and the phase velocity derivative with respect to frequency. In the first step, Hamilton's principle is applied to the Lagrangian density of the Rayleigh wave to deduce the fractional change in phase velocity at a given frequency

$$\begin{aligned} \left[\frac{\delta V_{ph}}{V_{ph}} \right]_{\omega} &= \frac{1}{4V_g V_{ph} I k^2} \left(\int_0^{\infty} \left(kr_1 + \frac{dr_2}{dz} \right)^2 \delta \Lambda dz \right. \\ &+ \int_0^{\infty} \left(2k^2 r_1^2 + 2 \left(\frac{dr_2}{dz} \right)^2 + \left(kr_2 - \frac{dr_1}{dz} \right)^2 \right) \delta \mu dz \\ &\left. - \int_0^{\infty} \left(\omega^2 (r_1^2 + r_2^2) \right) \delta \rho dz \right), \end{aligned} \quad (11)$$

with z being the depth, Λ and μ Lamé coefficients, $r_1(k, \omega, z)$ and $r_2(k, \omega, z)$ Rayleigh displacement vectors in the horizontal and vertical directions, respectively, and $I = \frac{1}{2} \int_0^{\infty} \rho (r_1^2 + r_2^2) dz$ the energy integral. Aki & Richards (2002) described the method used to calculate the partial derivative of the Love phase velocity with

respect to the medium parameter. Here, we perform the same work for the Rayleigh wave to obtain the following formulation:

$$\left[\frac{\partial V_{ph}}{\partial \Lambda} \right]_{\mu, \rho, \omega} = \frac{1}{4V_g I k^2} \left(kr_1 + \frac{dr_2}{dz} \right)^2, \quad (12)$$

$$\begin{aligned} \left[\frac{\partial V_{ph}}{\partial \mu} \right]_{\Lambda, \rho, \omega} &= \frac{1}{4V_g I k^2} \left[2k^2 r_1^2 \right. \\ &\left. + 2 \left(\frac{dr_2}{dz} \right)^2 + \left(kr_2 - \frac{dr_1}{dz} \right)^2 \right], \end{aligned} \quad (13)$$

$$\left[\frac{\partial V_{ph}}{\partial \rho} \right]_{\mu, \Lambda, \omega} = -\frac{1}{4V_g I k^2} \left(\omega^2 (r_1^2 + r_2^2) \right). \quad (14)$$

Given the equations of V_p , V_s as a function of Λ , μ , ρ : $V_p = \sqrt{(\Lambda + 2\mu)/\rho}$ and $V_s = \sqrt{\mu/\rho}$, the sensitivity of the Rayleigh phase velocity as a function of depth, that is, the partial derivatives of V_{ph} as a function of the medium's parameters (V_s , V_p and ρ) can be formulated as follows:

$$\left[\frac{\partial V_{ph}}{\partial V_p} \right]_{V_s, \rho, \omega} = \frac{V_p \rho}{2V_g I k^2} \left(kr_1 + \frac{dr_2}{dz} \right)^2, \quad (15)$$

$$\left[\frac{\partial V_{ph}}{\partial V_s} \right]_{V_p, \rho, \omega} = \frac{V_s \rho}{2V_g I k^2} \left[\left(kr_2 - \frac{dr_1}{dz} \right)^2 - 4kr_1 \frac{dr_2}{dz} \right], \quad (16)$$

$$\begin{aligned} \left[\frac{\partial V_{ph}}{\partial \rho} \right]_{V_p, V_s, \omega} &= \frac{V_p}{2\rho} \left[\frac{\partial V_{ph}}{\partial V_p} \right]_{V_s, \rho, \omega} + \frac{V_s}{2\rho} \left[\frac{\partial V_{ph}}{\partial V_s} \right]_{V_p, \rho, \omega} \\ &\quad - \frac{1}{4V_g I k^2} \omega^2 (r_1^2 + r_2^2). \end{aligned} \quad (17)$$

Since there is no analytical expression for group velocity sensitivity (Aki & Richards 2002), the sensitivity kernels for both the group velocity and the phase velocity derivative are calculated numerically. For group velocity, we use Taylor's theorem.

$$V_g(m) = V_g(m_0) + \left[\frac{\partial V_g}{\partial m} \right]_{m_0} (m - m_0) + h_1(m)(m - m_0), \quad (18)$$

with m representing the medium's parameters and $\lim_{m \rightarrow m_0} h_1(m) = 0$. Under this condition, we write

$$\left[\frac{\partial V_g}{\partial m} \right]_{m_0} = \frac{V_g(m) - V_g(m_0)}{m - m_0}. \quad (19)$$

For a given medium, the Rayleigh phase velocity can be expressed as a function of the frequency and the medium's parameters: $V_{ph} = f(\omega, V_s, V_p, \rho)$. The total derivative of the phase velocity is written as

$$dV_{ph} = \frac{\partial V_{ph}}{\partial \omega} d\omega + \sum \frac{\partial V_{ph}}{\partial m} dm \quad (20)$$

with m a vector of the medium parameters V_s , V_p and ρ , which are independent of frequency, we obtain:

$$\frac{dV_{ph}}{d\omega} = \frac{\partial V_{ph}}{\partial \omega} + \sum \frac{\partial V_{ph}}{\partial m} \frac{dm}{d\omega} = \frac{\partial V_{ph}}{\partial \omega}. \quad (21)$$

According to the symmetry of second derivatives in mathematics, we can write:

$$\frac{\partial}{\partial \omega} \left(\frac{\partial V_{ph}}{\partial m} \right) = \frac{\partial}{\partial m} \left(\frac{\partial V_{ph}}{\partial \omega} \right) = \frac{\partial}{\partial m} \left(\frac{dV_{ph}}{d\omega} \right). \quad (22)$$

Thus, the sensitivity kernel of the phase velocity derivative can be assessed numerically by calculating the gradient of $\partial V_{ph}/\partial m$ related to the frequency. The latter was calculated previously as the Rayleigh phase velocity sensitivity. The resulting sensitivity kernels for each inversion input data, that is, phase velocity, group velocity and its derivative, for the fundamental mode, are presented

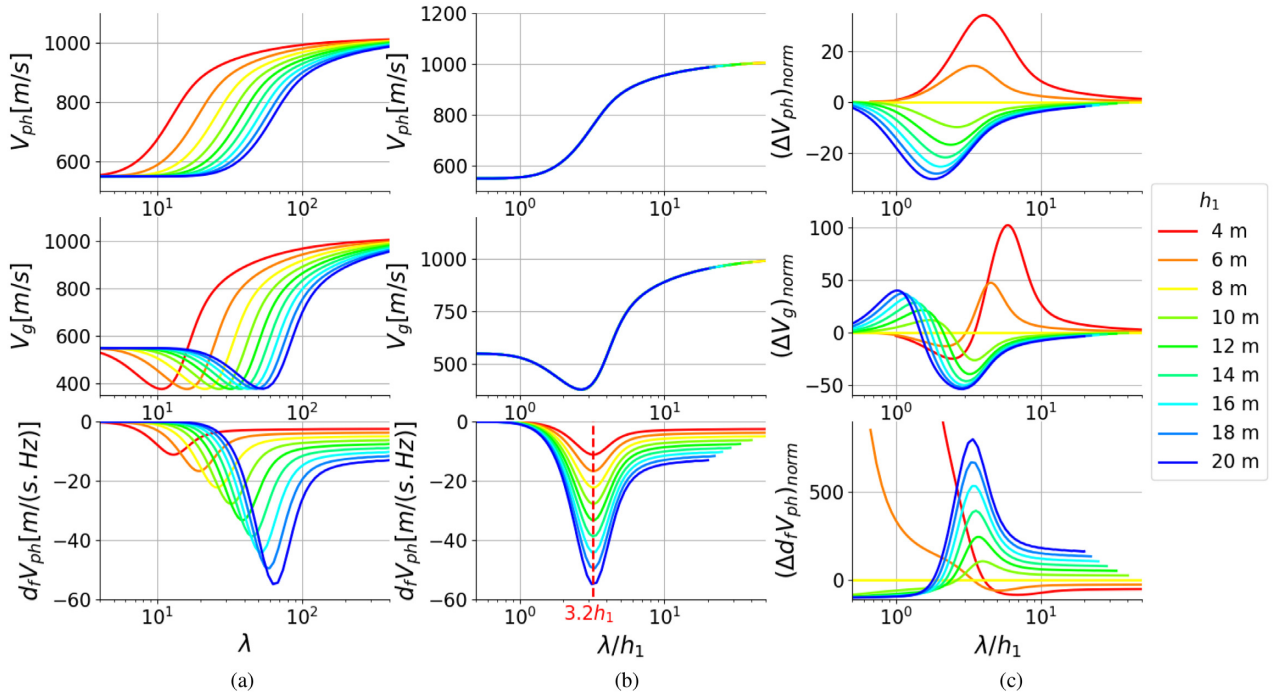


Figure 3. (a) Dispersion curves of the Rayleigh wave phase velocity (top), group velocity (middle) and phase velocity derivative (bottom) with depth variation $h_1 \in [4, 12]$ m, as a function of wavelength. (b) Dispersion curves as a function of normalized wavelength. (c) Normalized variations of the dispersion data.

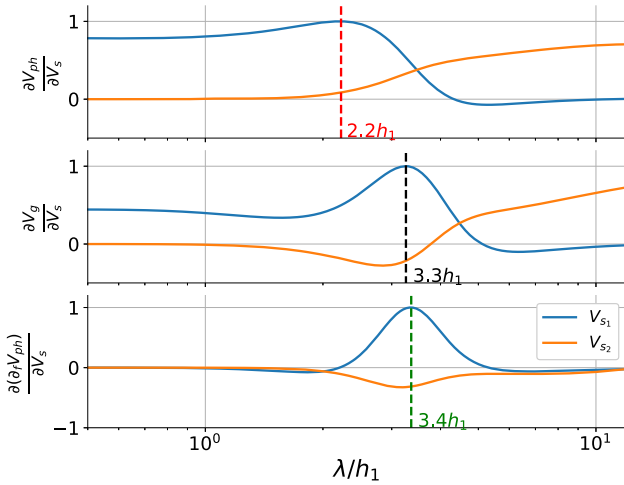


Figure 4. Rayleigh phase velocity sensitivity kernel (top), group velocity sensitivity kernel (middle) and phase velocity derivative sensitivity (below) with respect to the shear wave velocities of the shallow layer (V_{s_1}) and the deep layer V_{s_2} . Sensitivity values normalized by the maximum value of sensitivity with respect to V_{s_1} and presented as a function of wavelength normalized by the depth of the shallow layer h_1 .

in Fig. 4 as a function of normalized wavelength. Note that, as mentioned previously, for this study, the sensitivity is calculated and presented as related only to the shear wave velocity parameter. In Fig. 4, the blue curves show the sensitivity of the inversion input data to variations of shear wave velocity of the shallow layer (V_{s_1}) and orange curves show the shear wave velocity of the half-space V_{s_2} variations. To make the results comparable, all the curves are normalized by the maximum sensitivity value of each inversion input data.

In Fig. 4, it can be seen that with V_{s_1} variations, both V_{ph} and V_g , have high sensitivity values at short wavelength. However, when variations occur in the deep layer (V_{s_2}), it is necessary to have a long wavelength to obtain more sensitivity, but precise estimation of the medium is difficult due to high uncertainties (Lai *et al.* 2005). In contrast, the resulting sensitivity of the PVD is found to be significant at $\lambda \approx 3.4h_1$ for both V_{s_1} and V_{s_2} variations. From the standpoint of inversion, regarding this two-layer reference medium, this behaviour indicates that the shear wave velocity variations occurring in whichever layer can be estimated by the phase velocity derivative over a limited range of wavelengths, where the phase velocity derivative is sensitive.

The analysis of the sensitivity kernel in Fig. 4 is in good agreement with the previous qualitative analysis shown in Fig. 3. The maximum sensitivity and largest variations of the phase velocity derivative occur for the same order of wavelength ($\lambda \approx 3.4h_1$). In addition, the sensitivity kernels for models with different first layer depths (h_1) but with the same shear wave velocities are also calculated. The same conclusion as for the qualitative analysis is also found: the maximum sensitivity of the phase velocity derivative still occurs for $\lambda \approx 3.2h_1$, under the assumption of fixed model shear wave velocities.

5 INVERSION TESTS

In the previous two sections, we discussed the sensitivity of the PVD dV_{ph}/df both qualitatively and quantitatively. In this part, we apply dV_{ph}/df in a numerical inversion problem to verify its feasibility. Three types of dispersion data are taken as inversion input data: V_{ph} , V_g and dV_{ph}/df . For that, theoretical dispersion curves of V_{ph} and V_g are calculated using Geopsy software (Wathelet *et al.* 2004). The PVD is then calculated using eq. (8). Note that, since only the fundamental mode is tackled, the dispersion curve calculated is that of the fundamental mode only.

The parameters of the reference model are presented in Table 1 and we assume that the medium has undergone minor changes such that its shear wave velocities change with variation ratios $\alpha(V_{s_i}) \leq 5$ per cent. The dispersion curves are calculated for the reference model and the models with shear wave velocity variations in a frequency range [1, 160] Hz with a frequency sampling step of 0.5 Hz. This frequency band has been chosen for these inversion tests because it corresponds to that of an ideal pulse source centred on 50 Hz, this central value being itself typical of a hammer shot used in subsurface geophysics. Fig. 5 presents the dispersion curves of the three dispersion data, as function of frequency.

5.1 Misfit function and *a priori* information

The dispersion data are tested below for an inversion process by a global optimization through the NA, as indicated in Section 1: the NA computes the misfit function in the parameter space, where the pseudo-random samples are generated at each iteration by making use of Voronoi cells, and then guided and improved by the samples generated at the previous iteration. Each sample corresponds to one ground model (i.e. a set of the research parameters: V_s of each layer in the model) and corresponds to one calculated dispersion curve using Geopsy software. The objective (also called misfit) function is defined as the L2 norm relative difference between measured and calculated inversion data values, x_{mes} and x_{cal} respectively, in the frequency domain

$$\text{misfit} = \sqrt{\frac{1}{N_f} \sum_i^{N_f} \left(\frac{x_{mes} - x_{cal}}{x_{mes}} \right)^2}, \quad (23)$$

where N_f is the number of inversion input data in the frequency domain, x is the inversion input data, V_{ph} , V_g or dV_{ph}/df . We define an indicator function such that its value is between 0 and 1:

$$P = e^{-\text{misfit}}. \quad (24)$$

In our inversion, the compressional-wave velocity V_p , the first layer depth h_1 and the density ρ are fixed, only the shear wave velocities of both layers V_{s_i} are inverted and are searched in the domain $[-20 \text{ per cent}, +20 \text{ per cent}] \times V_{s_i}^{\text{ref}}$. NA needs several tuning parameters in an inversion process: $n_{s_0} = 50$ the number of samples randomly distributed in the parameter space as well as the Voronoi cells number at the initial iteration; $n_r = 5$ the number of best cells to consider for the next iteration; $n_s = 10$ the number of new generating samples at each selected cell; and $n_i = 15$ the total number of iteration. Finally, a total of 800 ($= n_{s_0} + n_r \times n_s \times n_i$) models are calculated in each inversion.

5.2 Inversion results of V_{ph} and V_g

Figs 6 and 7 present the inversion results of the phase velocity and the group velocity, respectively, with each dot corresponding to one inverted model. Black dots are inversion results for the reference medium ($\alpha = 0$) and blue dots are inverted models for the medium with the variation $\alpha > 0$, the red dots represent $\alpha < 0$. A maximum probability value of 99 per cent ($99\%P_{\text{max}}$) is used as a limit for all the inversion models in each inversion, which means only the models with $P \geq 0.99 P_{\text{max}}$ are selected as acceptable. In each figure, the top four images show the selected inversion results when small variations occur in the shallow medium ($\alpha(V_{s_1})$), and the bottom four correspond to the cases of small variations in the deep medium ($\alpha(V_{s_2})$).

For both the phase velocity and the group velocity (Figs 6 and 7), when small variations occur in the shallow medium ($\alpha(V_{s_1})$), those greater than 3 per cent can be well estimated because the inversion results can be clearly distinguished from those of the reference model. When the variation is equal to 2 per cent, the inversion results begin to overlap and when $\alpha(V_{s_1}) = 1$ per cent, the inversion results cannot be separated. For variations in the deep medium ($\alpha(V_{s_2})$), the inversion results overlap when $\alpha(V_{s_2}) = 4$ per cent. Therefore, in this two-layer medium, the classical inversion method can estimate variations of the shear wave velocity in the shallow medium which are greater than 3 per cent. However, for variations in the deep medium, only variations greater than 5 per cent can be estimated.

5.3 Inversion results of dV_{ph}/df

As shown in section 3, the qualitative analysis of the behaviour of the PVD, dV_{ph}/df tends to zero at high frequencies (short wavelengths) where the shear wave velocity variation is small (see Fig. 5), which causes the objective function to tend to infinity. Consequently, the inversion of dV_{ph}/df tends to find models that better fit the dispersion curves at high frequencies. To avoid this problem, we propose here to invert a combined dispersion curve by using the derivative of the dispersion velocity for lower frequencies and dispersion velocities for the higher frequencies. The frequency limit between the two ranges is chosen here in order to integrate the derivative of the phase velocity over a sufficiently wide range including the zone of maximum sensitivity. According to the sensitivity curves of dV_{ph}/df (Fig. 4), dV_{ph}/df is most sensitive when $\lambda \in [2, 6]h_1 = [16, 48]$ m, which corresponds to the frequency range [20, 40] Hz in the tested case. Thus, the combined dispersion curve is dV_{ph}/df when $f < 60$ Hz and V_{ph} when $f \geq 60$ Hz. Note that the frequency range limits for dV_{ph}/df have been chosen here by considering the part of the dispersion curves featuring the higher variations but it remains arbitrary. This choice for the limits values could be driven by a benchmark test approach in further studies with the objective to automatically recover the optimum values of the frequencies boundaries.

Fig. 8 shows that the combined data inversion has a quasi-equivalent estimation for the shallow layer V_{s_1} . But when variations occur in the deep medium, the inversion of the combined data better estimates small V_{s_2} variations. The normalized convergence curve of the indicator P in Fig. 9 shows that all inversion processes converge after around 300 iterations and the number of selected models for both inversions varies between [550, 650]. In order to obtain a clearer view of the selected models, they are presented quantitatively in Fig. 10.

The inversion results of the combined dispersion curve and V_{ph} are shown in Fig. 10: the inverted shear wave velocities are plotted as a function of the variation ratio α . The black line presents the expected values, and the coloured zones show, extreme inverted values for V_{ph} (red zone) and the combined dispersion curve (grey zone), respectively, which correspond to extreme V_s values in Fig. 8. The advantage of combined data inversion is obvious for V_{s_2} because the result area is narrower around the expected value. In the next section, the procedure is tested with real laboratory measurements.

6 APPLICATION ON REAL DATA FROM LABORATORY MEASUREMENTS

Two reduced-scale models made of epoxy resin (Fig. A1), were designed to validate and illustrate our results experimentally. The

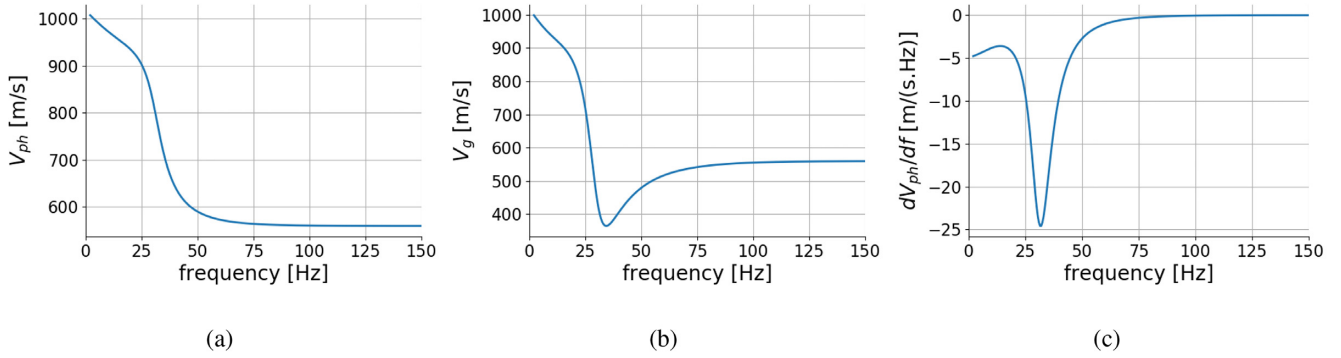


Figure 5. Theoretical dispersion curves of the reference medium (Table 1). (a) V_{ph} , (b) V_g and (c) dV_{ph}/df .

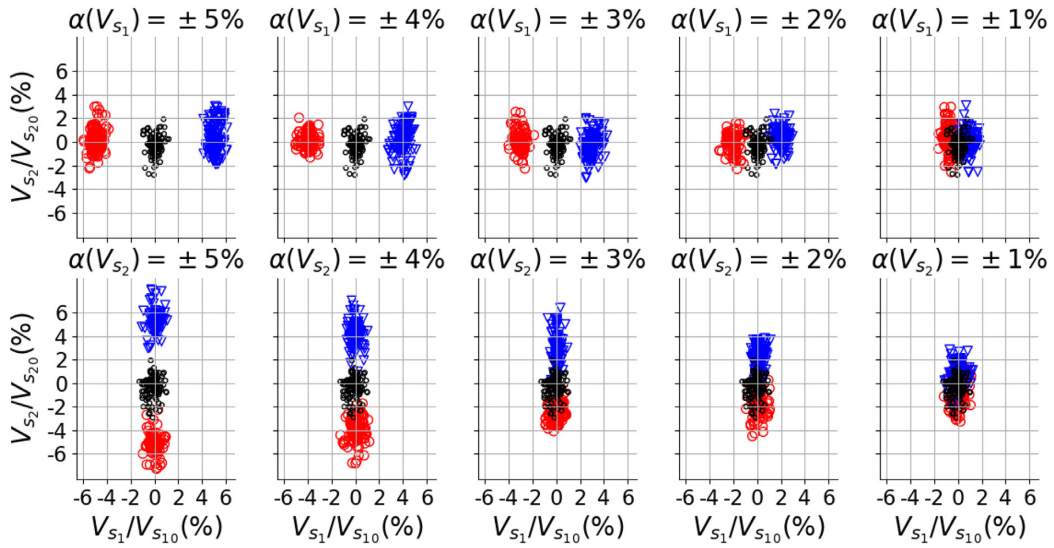


Figure 6. V_{ph} inversion results. Each dot corresponds to one inverted model with the colours representing reference and shear wave velocity variation media. Black: $\alpha(V_{s_i}) = 0$; red: $\alpha(V_{s_i}) < 0$; blue: $\alpha(V_{s_i}) > 0$.

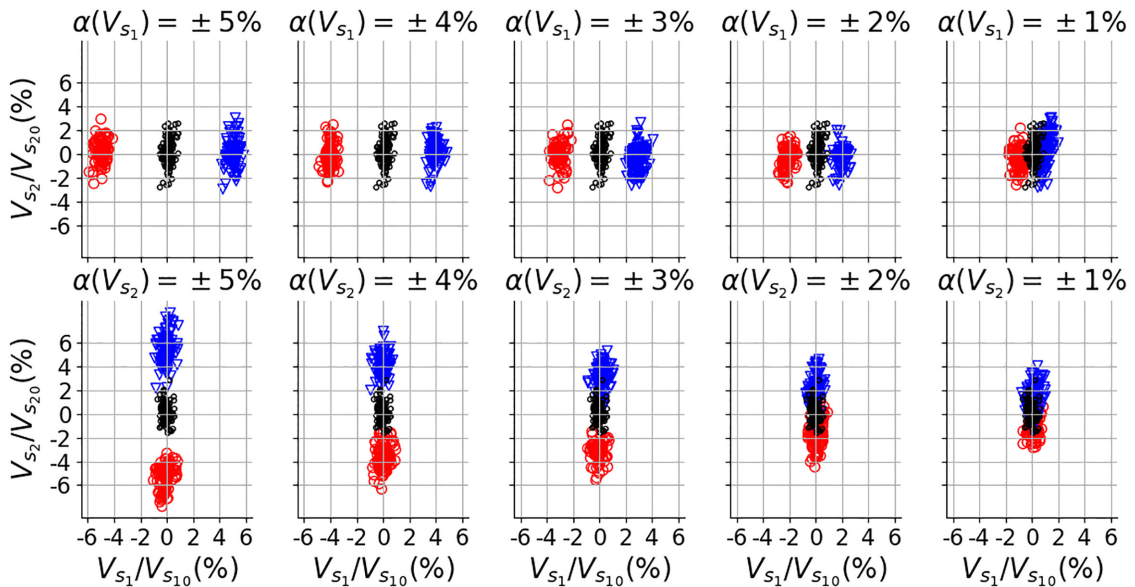


Figure 7. V_g inversion results. Each dot corresponds to one inverted model with the colours representing reference and shear wave velocity variation media. Black: $\alpha(V_{s_i}) = 0$; red: $\alpha(V_{s_i}) < 0$; blue: $\alpha(V_{s_i}) > 0$.

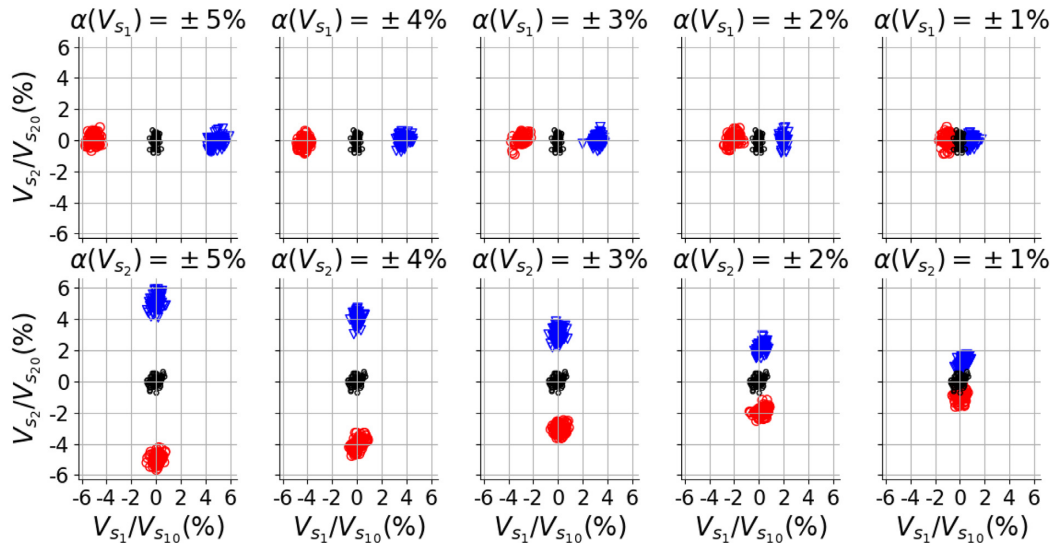


Figure 8. Combined data inversion results. Each dot corresponds to one inverted model with the colours representing reference and shear wave velocity variation media. Black: $\alpha(V_{s_i}) = 0$; red: $\alpha(V_{s_i}) < 0$; blue: $\alpha(V_{s_i}) > 0$.

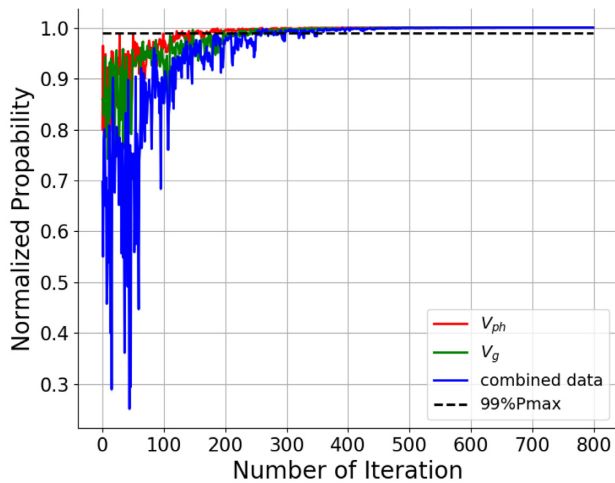


Figure 9. Normalized probability curves for V_{ph} , V_g and combined dispersion curves as function of iteration number.

parameters and dimensions of the first model (named *baseline*) are given in Table 2. Using the sample parameters provided by previous studies on this type of resin (Filippi *et al.* 2019), we calculated the size of the model to minimize and delay the boundary effects. Moreover, the latter are reduced because the borders of the models are rounded using a radius larger than or equal to the central wavelength (Pageot *et al.* 2015). The radius of the rounded borders is 12 mm ($r \approx V_R/f$) and is identical for both resin models. The second model (named *repeatline*) was similar to the first one but with a higher shear wave velocity in depth. The variation ratio is $\alpha(V_{s_2}) = 17$ per cent as $V_{s_2} = 1100 \text{ m s}^{-1}$ for the *repeatline* model (model parameters of the *repeatline* are available in Table A1 in Appendix A).

6.1 Model measurements

The measurements were conducted in the MUSC (Measurement at Ultrasonic Scale) laboratory which permits carrying out seismic analogical measurements at reduced scale (Bretaudeau *et al.* 2011).

The scale ratio between the numerical and experimental model dimensions is 1000, that is, 1 m in the numerical model is 1 mm in the laboratory model, and 1 Hz corresponds to 1 kHz (Pageot *et al.* 2017). A Ricker wavelet with a central frequency of 100 kHz was generated with a dry contact point piezoelectric transducer and the signals were recorded with a moving laser interferometer, with a sampling rate equal to 10 MHz (see Fig. A1a in Appendix A for an illustration of the experimental set-up). More specifications of the MUSC measurement bench are available in (Bretaudeau *et al.* 2011) for any reproduction of the experiment. Fig. A1(b) in Appendix A shows the position of the piezo-electric source and the measurement points of the laser receivers (maximum offset equal to 90 mm with a space of 1 mm). Like all the recordings published from the MUSC bench, the measurements are available to the scientific community and can be obtained as free data on request by email.

Seismograms measured on the two models were then analysed and processed. Fig. 11(a) shows the measured *baseline* and *repeatline* seismograms. The phase velocity dispersion diagrams are extracted from the measured seismograms, using the phase-shift method (Fig. 11b). The dispersion diagrams are calculated in the frequency range [10, 150] Hz and at each frequency, the phase velocity is searched in the velocity range [500, 1500] m s^{-1} with the velocity resolution equal to 2 m s^{-1} . They are then normalized by the maximum value at each frequency and the value of the contour line plotted is 0.5. The difference is visible between the diagrams at low frequency, which corresponds to velocity variations in the deep layer. The V_{ph} dispersion curves are then extracted by automatic picking and their gradients give the dV_{ph}/df dispersion curves (Fig. 12).

It should be pointed out that the PVD is extracted here using the gradient of the measured phase velocity curve instead of using the group velocity as proposed in eq. (8). As the matter of fact, the high contrast of the shear wave velocity between the two layers, which gives a very steep variation of the group velocity as a function of frequency (i.e. a high dispersion), makes the choice of the frequency filter range, in the MFM procedure described in introduction, too difficult for accurately defining the group velocity required in eq. (8) for dV_{ph}/df . Indeed, a wide frequency range can bias the central

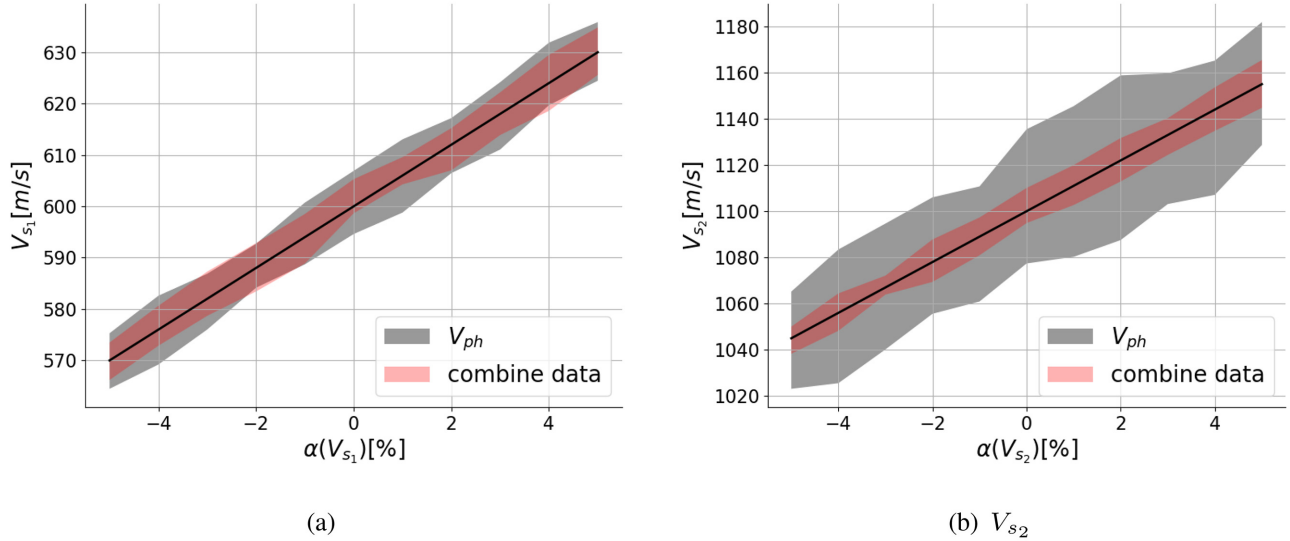


Figure 10. Inversion results of shear wave velocities for (a) shallow layer V_{s1} and (b) deep layer V_{s2} , using V_{ph} and dV_{ph}/df separately. The black line presents the exact shear wave velocity value for each variation ratio α .

Table 2. Baseline model parameters and dimensions. h_i : layer thickness; l and w : length and width of model. Scale ratio between the numerical and the experimental model dimensions is 1000.

Layer	V_{pi} (m s ⁻¹)	V_{si} (m s ⁻¹)	ρ_i (kg m ⁻³)	ν_i	h_i (mm)	l (mm)	w (mm)
1	1300	703	450	0.29	8.0	265	235
2	2048	933	1300	0.37	203	265	235

frequency where the group velocity is searched; on the contrary, a narrow frequency range cannot contain enough energy to estimate the group velocity properly. This critical point of the group velocity assessment, above the scope of this study, should be tackled in further approaches, as mentioned in the final discussion of this paper.

As previously stated, only the fundamental mode is inverted. The cut-off frequency at high frequencies is fixed at 90 kHz to avoid the higher mode perturbation for both baseline and repeatline models. The signals at low frequency (below 35 kHz), which presents a low signal-to-noise ratio and requires unavailable large receiver offset to be correctly assessed and mitigate the near field effects as highlighted by Bodet *et al.* (2009), who recommend a minimum frequency such as the maximum wavelength is lower than half of the receiver offset, are not used. According to these criteria, in the following, the frequency band is chosen in [35, 90] Hz for both models. See Fig. A2 for a better visualization. However, as mentioned in the previous part concerning the theoretical tests, a further study should deal with the frequencies boundaries that can be automatically defined for optimal results.

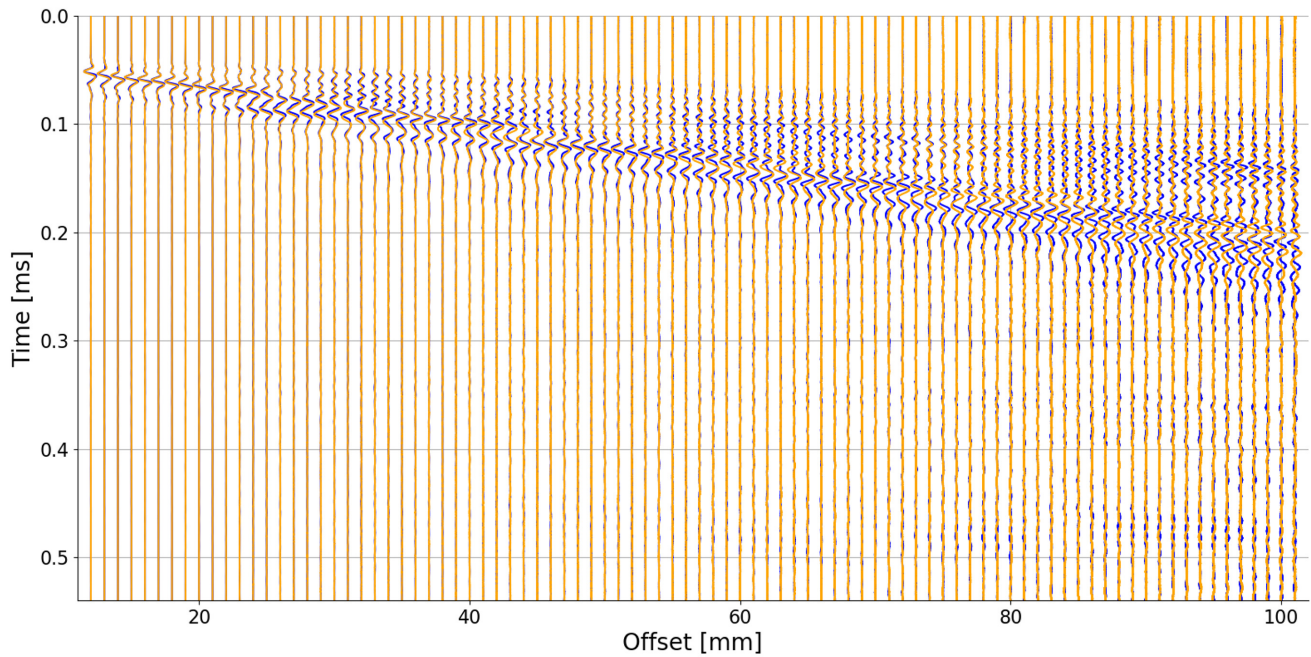
The PVD dV_{ph}/df and the classical dispersion data V_{ph} are now inverted to perform an accurate evaluation of the difference between the two models. As in Section 5, the inversions are carried out using V_{ph} and combined dispersion curves. The combined dispersion curve consists of dV_{ph}/df at medium frequencies ($f \in [42, 70]$ Hz) and V_{ph} at low and high frequencies ($f \in [35, 42] \cup [70, 90]$ Hz). These limits are defined to avoid both an oscillation effect at low frequencies and a normalization problem at high frequencies. In the following, we invert the dV_{ph}/df dispersion curve, without the normalization in the misfit function, and discuss its robustness.

6.2 Inversion results

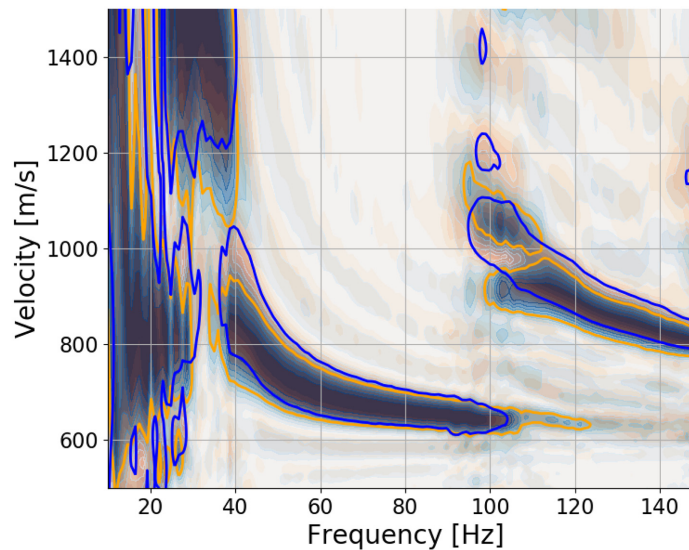
In the Neighborhood Algorithm inversion process, we consider the compressional-wave velocity and density set as provided in Table 2. The shear wave velocities of each layer are searched in the range $V_{s1} \in [500, 900]$ m s⁻¹, $V_{s2} \in [800, 1200]$ m s⁻¹ and in the depth of the first layer in the range $h_1 \in [7.2, 8.8]$ m. Fig. 13 shows the resulting couples of shear wave velocities (V_{s1} , V_{s2}) recovered by all the inversion processes, where V_{s1} and V_{s2} correspond to the shallow and deep layer, respectively. The results are shown for all three inversions: solely V_{ph} , solely dV_{ph}/df , combined V_{ph} and dV_{ph}/df curves. There are 1520 models ($n_{s0} = 20$, $n_r = 10$, $n_s = 10$, $n_i = 20$) in each inversion process and the convergence indicator curves are plotted in Fig. 14. The convergence curves of V_{ph} and combined data inversions tend towards the same level but reach a lower value for dV_{ph}/df because of the non-normalization in the misfit function.

The result scatter plots in Fig. 13 focus more on the true value on the V_{s1} axis when V_{ph} is considered for the inversion than when it is for the other inversion data. However, dV_{ph}/df and the combined data inversions give better estimations on V_{s2} , as we can see better discrimination between the results of the baseline and repeatline models. To analyse the inversion results quantitatively, histograms of inverted models are shown in Fig. 15, as a function of inverted V_{s1} and V_{s2} , separately. μ_b and σ_r are mean values and standard deviations for each group of models where ‘b’ represents the baseline and ‘r’ the repeatline. As there is no variation in the shallow layer between *baseline* and *repeatline*, the two inverted V_{s1} should be identical.

Compared to dV_{ph}/df and combined data inversion, V_{ph} inversion provides inverted V_{s1} values with smaller standard deviations for both *baseline* and *repeatline*, which corresponds to the more focused



(a)



(b)

Figure 11. (a) Measured seismograms for the baseline model (orange) and the repeatline model (blue), normalized by maximum values at each trace. (b) Dispersion diagrams for the baseline model (orange) and the repeatline (blue), normalized by the maximum value at each frequency. The value of the contour line is equal to 0.5. The measured seismograms and the dispersion diagrams are presented separately in Fig. A2 for a clear display of each one.

results in Fig. 13. In Fig. 15(a), the two histograms of combined data inversion are superimposed but the differences between μ_b and μ_r are significant due to several bigger inverted V_{s1} values of the repeatline (the part between 710 and 750 m s^{-1}).

The assessment of the deep layer variation is presented in Fig. 15(b). The variation ratio $\alpha(V_{s2})$ is equal to 16.0 ± 0.7 per cent for V_{ph} alone, 16.4 ± 1.1 per cent for dV_{ph}/df alone and 17.1 ± 0.3 per cent for combined data inversions. The result of V_{ph} is smaller than the reference value 17 per cent, and the error of the dV_{ph}/df

inversion result is larger than that of the other two inversions. The result of the combined data inversion is not only the closest to the expected reference value but it also has the smallest error. The improvement of the combined approach on the experimental data may seem small. However, the relative error with respect to the true model is divided by 2 and 6 depending on the data set, and the standard deviation is divided by 1.7 in both cases.

Using the mean values of the inverted models in Fig. 15, the calculated dispersion curves and the measured dispersion curves

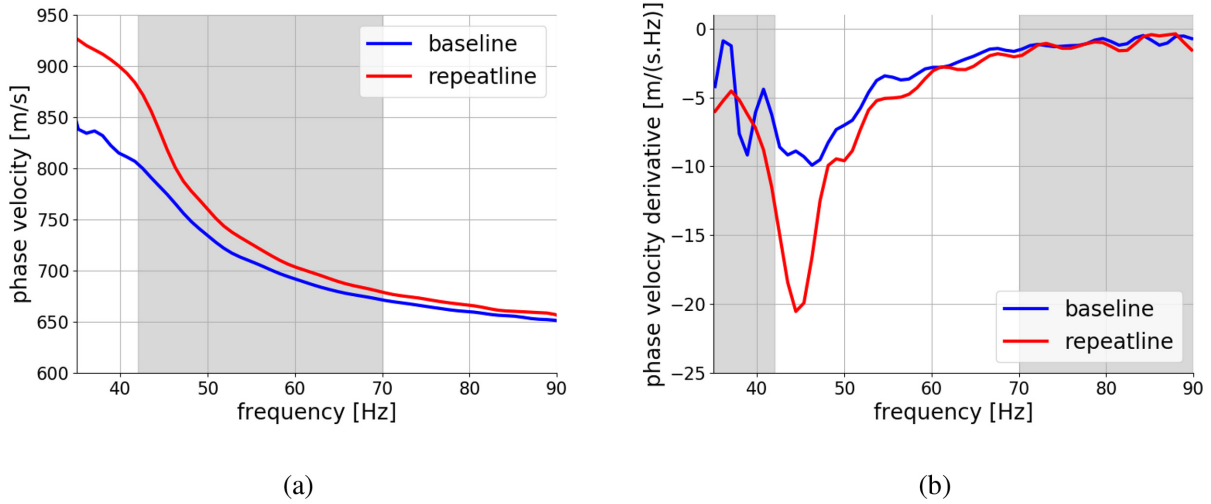


Figure 12. Measured dispersion curves of (a) the phase velocity V_{ph} and (b) the phase velocity derivative dV_{ph}/df . The combined data of *baseline* and *repeatline* consist of non-grey parts of the blue and red curves in the two images, respectively.

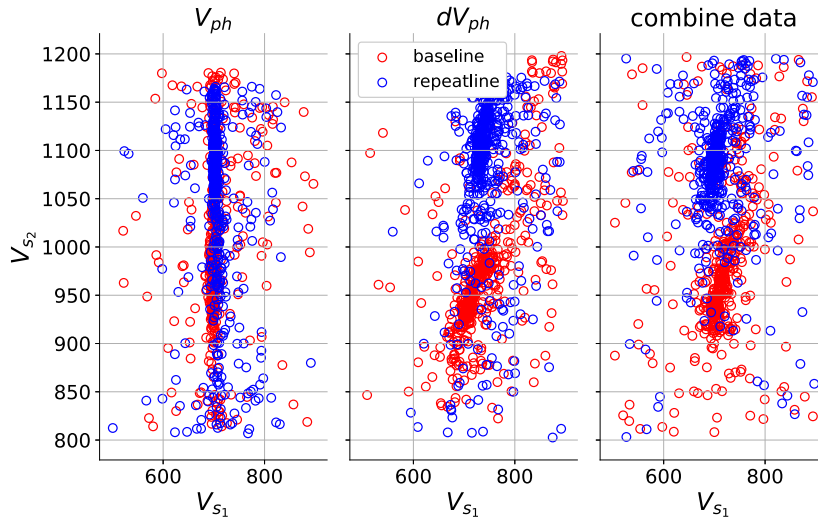


Figure 13. Inversion results of baseline (red) and repeatline (blue).

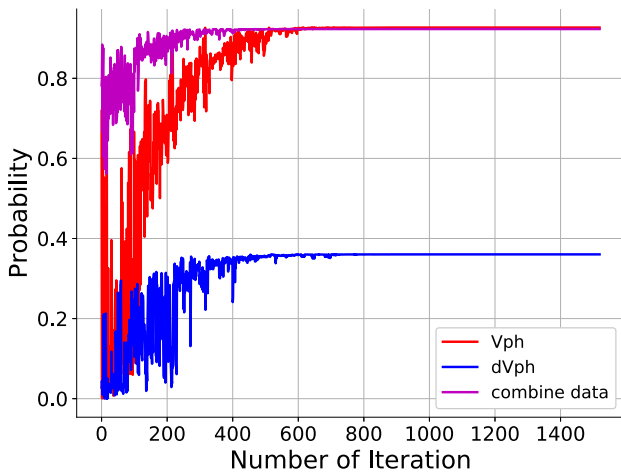
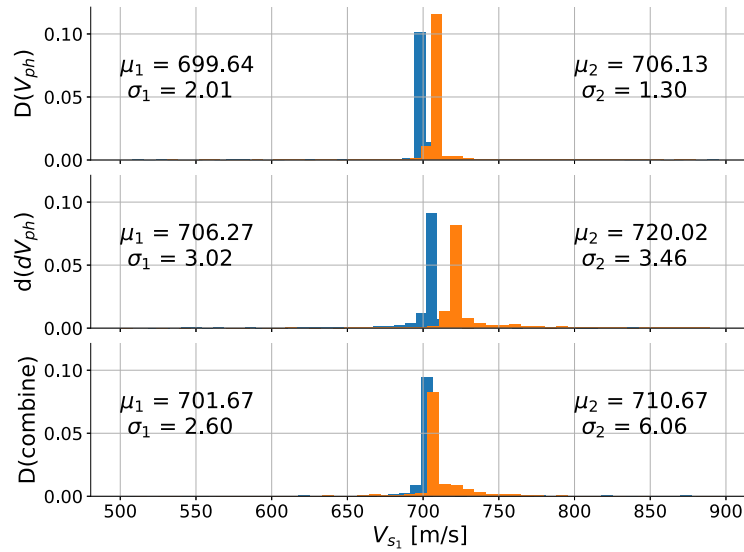


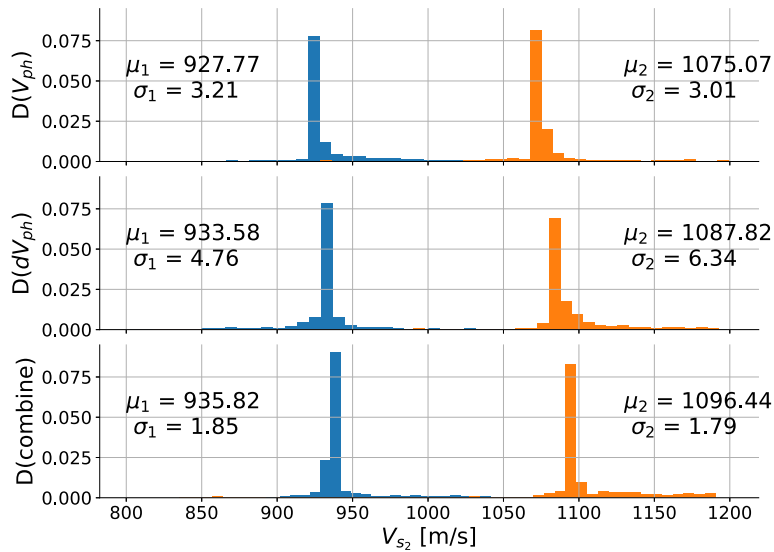
Figure 14. Probability curves for baseline inversion using V_{ph} , dV_{ph}/df and combined dispersion curves, respectively.

are plotted for the baseline and the repeatline in Fig. 16. We can see that the dispersion curve calculated from the inversion results of dV_{ph}/df is wholly above the measured curves, in both Figs 16(a) and (b) although their corresponding derivative curves fit well with the trend measured in (c) and (d). Indeed, two "parallel" dispersion curves share one gradient curve, which means using only dV_{ph}/df for the optimization search in the inversion process can result in the identification of several solutions that do not correspond to the real model. The combined data method avoids this problem since V_{ph} replaces dV_{ph}/df at both low and high frequencies. Thus, when using the combined data in inversion, both the high sensitivity of dV_{ph}/df and the calibration value to V_{ph} are taken into account. The results of the combined data inversion in Figs 16(c) and (d) are closer to the minimum values of the measured curves.

Viewed globally it should be noted that the MASW approach involves several steps regarding the overall indeterminacy of the method: the measurements and their uncertainties, the extraction of the dispersion data, the convergence of the inversion process according to the criterion of the cost function and the inversion input data and its sensitivity. This study proposed to explore the effects



(a)



(b)

Figure 15. Density histograms of baseline (blue) and repeatline (orange) inverted models as a function of (a) V_{s1} and (b) V_{s2} . The surface of each histogram is equal to 1.

of introducing the derivative of the Rayleigh wave phase velocity (PVD) in the process, independently of the issue of the measurement errors. Indeed, dissociating the effects of the different key elements of the process is crucial for the first stage. However further works will attempt to associate the effects of the measurements errors in order to identify their impacts. Thus, integrating the effect of errors on the data will contribute to the feasibility of the method in specific cases.

7 CONCLUSION AND DISCUSSION

In this paper, the derivative of the Rayleigh wave phase velocity $\frac{dV_{ph}}{df}$ is introduced in the surface wave inversion method, to estimate small variations in media (variation ratio smaller than 10 per cent). Based

on two-layer media, we discussed the performance of the PVD when small variations occur in both layers, in particular shear wave velocity variations. In the qualitative analysis, the dispersion curves of V_{ph} , V_g and dV_{ph}/df were calculated theoretically for several series of two-layer media with variations of shear wave velocities and the depth of the shallow layer. dV_{ph}/df displayed greater sensitivity compared to the phase and group velocities, especially for the deep layer variations: for the deep layer when the shear wave velocity variation was equal to 5 per cent, the variation of dV_{ph}/df was around 18 per cent while it was only 5 per cent for V_{ph} and V_g . Then, in the quantitative analysis, the calculation of sensitivity curves confirmed that dV_{ph}/df contained information from both layers when $\lambda \approx 3.4h_1$. As a reminder, the sensitivity of V_{ph} and V_g follows the following rule: a variation of the shallow layer provided high sensitivity at

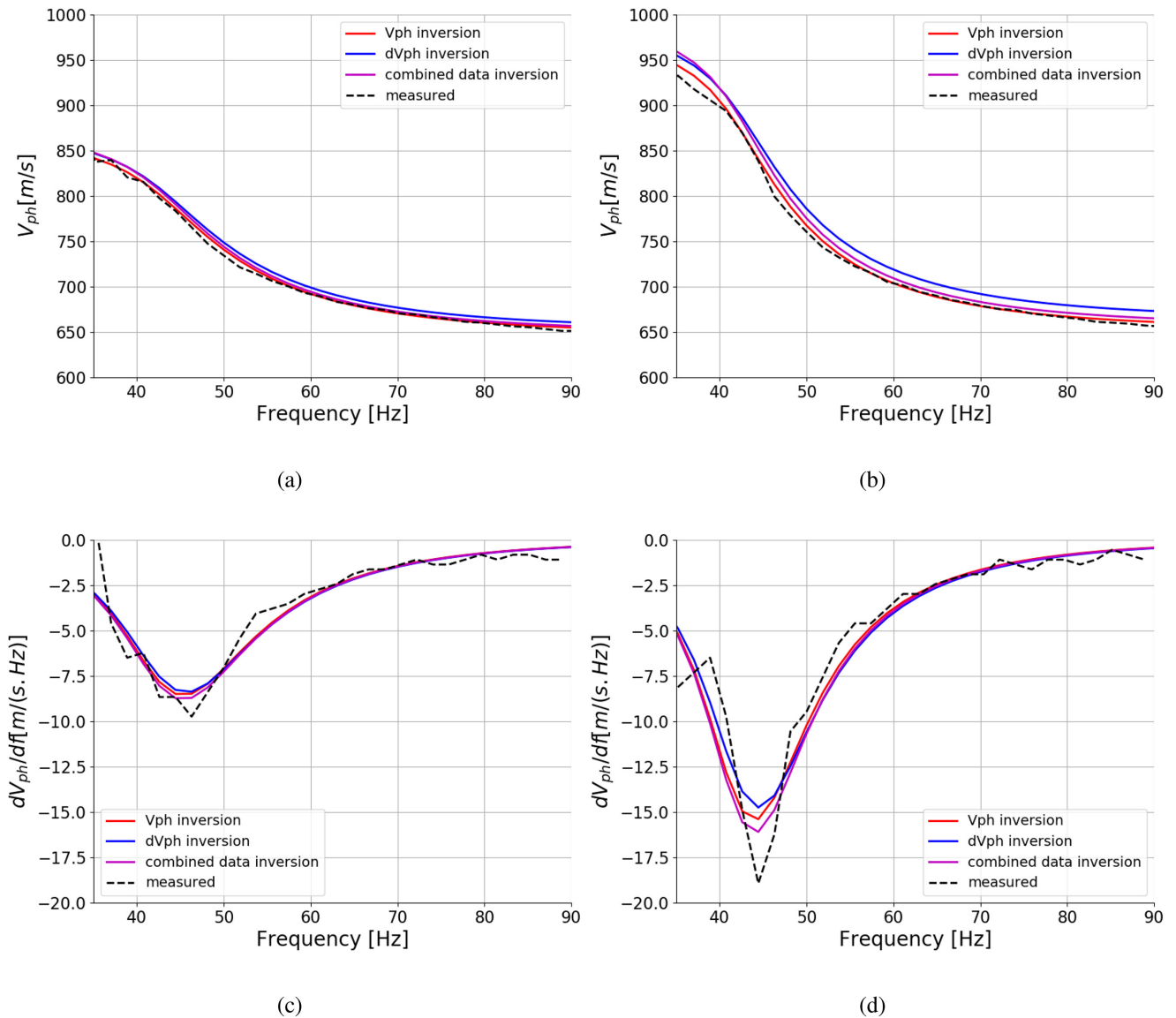


Figure 16. Phase velocity dispersion curves for the measured data of (a) *baseline* and (b) *repeatline*, and their corresponding inverted models from different inversion data. Phase velocity derivative dispersion curves for the measured data of (c) *baseline* and (d) *repeatline*, and their corresponding inverted models.

a short wavelength while a long wavelength was needed for high sensitivity to variation in the deep layer.

The feasibility of using dV_{ph}/df was then verified numerically by inverting the dispersion curves calculated from synthetic noisy signals. The high sensitivity of dV_{ph}/df was particularly interesting but it should be used with care in the inversion process, due to its high oscillation in the case of noise and to the derivative property which leads to confusion with the V_{ph} curves that share the same gradient in the frequency domain. To avoid this problem, we proposed to use combined data that consists of V_{ph} and dV_{ph}/df . We verified that the combined data contained both the high sensitivity of dV_{ph}/df and the robustness of V_{ph} at the same time. Then, two two-layer models made of resin-epoxy were used to illustrate this result experimentally. The difference between them was a 17 per cent variation of shear wave velocity in the deep layer. The V_{ph} inversion estimated the variation of the deep layer at (16.4 ± 1.1) per cent while the combined data inversion estimated the variation of the medium at (17 ± 0.3) per cent. Moreover, regarding the expected velocity values

of the deep layer, the combined method gives more precise results with a smaller error, which are divided by 1.9 and 6.9 depending on the data set as well as standard deviations divided by 1.7. This improvement makes sense when looking at changes in media for small variations such as in continuous monitoring.

The methodology proposed, which combined the two inversion data, used the performance of each one valid over distinct frequency ranges, and combined them over the whole frequency range of the measured data. The results showed that it is an appropriate inversion strategy because it allows using the phase velocity derivative over the frequency range for which it is most sensitive. We proposed to define this frequency range according to the feature of the phase velocity derivative: its use was limited to the part for which it presented a minimum, without taking into account the areas for which the result of the calculation showed strong oscillations at lower frequencies or the plateau area for the higher frequencies. However, this criterion remained qualitative here and could be the subject of further studies in the near future. It will also be interesting to analyse the behaviour

of the PVD for higher modes. Indeed, the experiments, which were carried out on two-layer epoxy resin models, confirmed that dV_{ph}/df is complementary to V_{ph} in the inversion. Work is now in progress using epoxy resin models with smaller variations of mechanical properties, and time-lapse inversion.

Moreover, other major points should be investigated in further studies: the experimental tests in the last part on real measurements have highlighted the complexity of using the low-frequency signal. The dispersion uncertainties for the lowest frequencies in the case of subsurface measurements are due, on the one hand, to the effects of near fields and, on the other hand, to the ratio between phase shift and wavelength (Bodet *et al.* 2009). Therefore, we propose, for future studies, to characterize all the uncertainties, including those for lower frequencies, for the phase velocity but also for the calculation of its derivative. The range of uncertainty for each frequency can be linked to the width of the lobe envelope associated with the fundamental mode in the dispersion diagram. The limits of this lobe can be computed analytically as proposed by (Wang *et al.* 2020). Derivatives of these limits as a functions of frequency, also analytically available, could identify the uncertainty associated with the phase velocity derivative. The effects of these uncertainties on inversion by the method proposed in this article could be further addressed by including it in the misfit weighting.

Finally, in the experimental tests, the phase velocity derivative was calculated by the gradient of the phase velocity and not by eq. (8) which uses the group velocity. The latter is indeed very difficult to evaluate in a robust way when the contrast between the two media is strong and implies a high-velocity dispersion: in this case, the choice of the filter width is critical and beyond the scope of the present study. Therefore, we propose, for future studies, to analyse the impact of the velocities contrast on the choice of this filter and the values from which assessment of the phase velocity derivative is more interesting by calculating the phase velocity gradient.

ACKNOWLEDGEMENTS

We would like to thank M. Wathelet, the co-developer of the *Geopsy* software. Our thanks are also extended to D. Pageot, G. Gugole and T. Devie for their help with the experimental measurements and data management. This work was co-funded by University Gustave Eiffel and the Région Pays de la Loire. Finally, we would like to thank J. Virieux for an informal discussion which gave birth to the idea of this innovative approach.

REFERENCES

- Aki, K. & Richards, P., 2002. *Quantitative Seismology*, 2nd edn, University Science Books.
- Auger, F. & Flandrin, P., 1995. Representations by the reassignment method, *IEEE Trans. Signal Process.*, **43**(5), 1068–1089.
- Bhattacharya, S.N., 2015. Sensitivities of surface wave velocities to the medium parameters in a radially anisotropic spherical Earth and inversion strategies, *Ann. Geophys.*, **58**(5), doi:10.4401/ag-6806.
- Bodet, L., Abraham, O. & Clorennec, D., 2009. Near-offset effects on Rayleigh-wave dispersion measurements: physical modeling, *J. Appl. Geophys.*, **68**(1), 95–103.
- Brethedeau, F., Leparoux, D., Durand, O. & Abraham, O., 2011. Small-scale modeling of onshore seismic experiment: a tool to validate numerical modeling and seismic imaging methods, *Geophysics*, **76**(5), T101–T112.
- Dangard, M., Bodet, L., Pasquet, S., Thiesson, J., Guérin, R., Jougnot, D. & Longuevergne, L., 2018. Estimating picking errors in near-surface seismic data to enable their time-lapse interpretation of hydrosystems, *Near Surf. Geophys.*, **16**(6), 613–625.
- Dunkin, J.W., 1965. Computation of modal solutions in layered, elastic media at high frequencies, *Bull. seism. Soc. Am.*, **55**(2), 335–358.
- Dziewonski, A., Bloch, S. & Landisman, M., 1969. A technique for the analysis of transient seismic signals, *Bull. seism. Soc. Am.*, **59**(1), 427–444.
- Filippi, C., Leparoux, D., Grandjean, G., Bitri, A. & Cte, P., 2019. New robust observables on Rayleigh waves affected by an underground cavity: from numerical to experimental modelling, *Geophys. J. Int.*, **218**(3), 1903–1918.
- Foti, S., Lai, C., Rix, G. & Strobbia, C., 2014. *Surface Wave Methods for Near-Surface Site Characterization*, CRC Press.
- Foti, S., *et al.*, 2018. Guidelines for the good practice of surface wave analysis: a product of the InterPACIFIC project, *Bull. Earthq. Eng.*, **16**, 2367–2420.
- Foti, S., Lancellotta, R., Sambuelli, L. & Socco, L.V., 2000. Notes on fk analysis of surface waves, *Ann. Geophys.*, **43**, doi:10.4401/ag-3683.
- Gabriels, P., Snieder, R. & Nolet, G., 1987. In situ measurements of shear-wave velocity in sediments with higher-mode Rayleigh waves, *Geophys. Prospect.*, **35**(2), 187–196.
- Gilbert, F. & Backus, G.E., 1966. Propagator matrices in elastic wave and vibration problems, *Geophysics*, **31**(2), 326–332.
- Haskell, N.A., 1953. The dispersion of surface waves on multilayered media, *Bull. seism. Soc. Am.*, **43**(1), 17–34.
- Joubert, A., Le Feuvre, M. & Côte, P., 2018. Passive monitoring of a sea dike during a tidal cycle using sea waves as a seismic noise source, *Geophys. J. Int.*, **214**(2), 1364–1378.
- Kodera, K., De Villedary, C. & Gendrin, R., 1976. A new method for the numerical analysis of non-stationary signals, *Phys. Earth planet. Inter.*, **12**(2–3), 142–150.
- Lai, C.G. & Rix, G.J., 1998. Simultaneous inversion of Rayleigh phase velocity and attenuation for near-surface site characterization, *PhD thesis*, Georgia Institute of Technology.
- Lai, C.G., Foti, S. & Rix, G.J., 2005. Propagation of data uncertainty in surface wave inversion, *J. Environ. Eng. Geophys.*, **10**(2), 219–228.
- Le Feuvre, M., Joubert, A., Leparoux, D. & Côte, P., 2015. Passive multi-channel analysis of surface waves with cross-correlations and beamforming. Application to a sea dike, *J. Appl. Geophys.*, **114**, 36–51.
- Luo, Y., Xia, J., Miller, R.D., Xu, Y., Liu, J. & Liu, Q., 2008. Rayleigh-wave dispersive energy imaging using a high-resolution linear radon transform, *Pure appl. Geophys.*, **165**(5), 903–922.
- McMechan, G.A. & Yedlin, M.J., 1981. Analysis of dispersive waves by wave-field transformation, *Geophysics*, **46**(6), 869–874.
- Métais, V., 2016. *Auscultation avec les ondes de surface de matériaux très hétérogènes*, *PhD thesis*, The French Institute of Science and Technology for Transport, Development and Networks, defended at University of Nantes, France.
- Mokhtar, T.A., Herrmann, R. & Russell, D., 1988. Seismic velocity and Q model for the shallow structure of the Arabian shield from short-period Rayleigh waves, *Geophysics*, **53**(11), 1379–1387.
- O'Neill, A., 2004. Shear velocity model appraisal in shallow surface wave inversion, in *Symposium on the Application of Geophysics to Engineering and Environmental Problems 2004*, pp. 1544–1555, Society of Exploration Geophysicists, doi:10.3997/2214-4609-pdb.186.SUR02.
- Pageot, D., Leparoux, D., Durand, O., Le Feuvre, M., Côte, P. & Capdeville, Y., 2015. Refined experimental studies for improving the reduced-scale physical modeling of seismic subsurface measurement, in *Near Surface Geoscience 2015-21st European Meeting of Environmental and Engineering Geophysics*, doi:10.3997/2214-4609.201413763.
- Pageot, D., Leparoux, D., Le Feuvre, M., Durand, O., Côte, P. & Capdeville, Y., 2017. Improving the seismic small-scale modelling by comparison with numerical methods, *Geophys. J. Int.*, **211**(1), 637–649.
- Park, C.B., Miller, R.D. & Xia, J., 1998. Imaging dispersion curves of surface waves on multi-channel record, in *SEG Technical Program Expanded Abstracts*, pp., 1377–1380.
- Pasquet, S., Bodet, L., Bergamo, P., Guérin, R., Martin, R., Mourgues, R. & Tournat, V., 2016. Small-scale seismic monitoring of varying water levels in granular media, *Vadose Zone J.*, **15**(7), doi:10.2136/vzj2015.11.0142.

- Pedersen, H.A., Mars, J.I. & Amblard, P., 2003. Improving surface-wave group velocity measurements by energy reassignment, *Geophysics*, **68**(2), 677–684.
- Planès, T., Mooney, M.A., Rittgers, J. B.R., Parekh, M.L., Behm, M. & Snieder, R., 2016. Time-lapse monitoring of internal erosion in earthen dams and levees using ambient seismic noise, *Géotechnique*, **66**(4), 301–312.
- Planès, T., Rittgers, J.B., Mooney, M.A., Kanning, W. & Draganov, D., 2017. Monitoring the tidal response of a sea levee with ambient seismic noise, *J. Appl. Geophys.*, **138**, 255–263.
- Sambridge, M., 1999. Geophysical inversion with a neighbourhood algorithm—II. Appraising the ensemble, *Geophys. J. Int.*, **138**(3), 727–746.
- Socco, L. & Strobbia, C., 2004. Surface-wave method for near-surface characterization: a tutorial, *Near Surf. Geophys.*, **2**, 165–185.
- Socco, L.V., Foti, S. & Boiero, D., 2010. Surface-wave analysis for building near-surface velocity models—established approaches and new perspectives, *Geophysics*, **75**(5), 75A83–75A102.
- Takeuchi, H., Saito, M. & Bolt, B., 1972. Seismic surface waves, *Methods Comput. Phys.*, **11**, 217–295.
- Thomson, W.T., 1950. Transmission of elastic waves through a stratified solid medium, *J. Appl. Phys.*, **21**(2), 89–93.
- Wang, A., Le Feuvre, M., Leparoux, D. & Abraham, O., 2018. Impact of small shear wave velocity variations on surface wave phase velocity inversion, in *24th European Meeting of Environmental and Engineering Geophysics*, European Association of Geoscientists & Engineers, 1–5.
- Wang, A., Leparoux, D., Abraham, O. & Le Feuvre, M., 2019. Evaluation of dispersion diagrams distances based on usual histogram analysis for the surface wave difference inversion, in *1st Conference on Geophysics for Infrastructure Planning, Monitoring and BIM*, European Association of Geoscientists & Engineers, 1–5.
- Wang, A., Leparoux, D. & Abraham, O., 2020. Differential inversion of surface wave methods: proposition of diagram distance as inversion data, in *26th European Meeting of Environmental and Engineering Geophysics*, European Association of Geoscientists & Engineers, 1–5.
- Wathelet, M., 2008. An improved neighborhood algorithm: parameter conditions and dynamic scaling, *Geophys. Res. Lett.*, **35**(9), doi:10.1029/2008GL033256.
- Wathelet, M., Jongmans, D. & Ohrnberger, M., 2004. Surface-wave inversion using a direct search algorithm and its application to ambient vibration measurements, *Near Surf. Geophys.*, **2**, 211–221.
- Xia, J., 2014. Estimation of near-surface shear-wave velocities and quality factors using multichannel analysis of surface-wave methods, *J. Appl. Geophys.*, **103**, 140–151.
- Yilmaz, O., 2001. *Seismic data analysis: Processing, inversion, and interpretation of seismic data*, Society of exploration geophysicists.

APPENDIX A: TWO-LAYER RESIN MODELS AND EXPERIMENTAL SET-UP

The two resin models are presented in Fig. A1(a). The experimental set-up consists of a piezo-electric transducer (Fig. A1b) as a point source and a laser interferometer to measure the wave propagation (Fig. A1c). For the experimental tests, the piezo-electric source is fixed on the horizontal harm visible in Fig. A1(c) below the laser interferometer. Fig. A1 (d) provides information on the positions of the source and the receivers, with the dimensions of the resin models.

The model parameters of the baseline are available in Table 2. The models consist of two superimposed plates. The pink upper part is machined in a layer of industrial epoxy resin (polyurethane). The lower part is molded underneath this plate from an epoxy resin mixture (casting polyurethane) with an additional filler (hydrated alumina) which gives it specific V_s velocity properties. The choice of the amount of filler included in the polymerized mixture was decided on the basis of information provided in previous experimental studies (Pageot *et al.* 2015; Métails 2016; Filippi *et al.* 2019). The filled resins finally used in this study were also tested by independent measurements. The parameters of the repeatline model are given in Table A1. Fig. A2 presents separately the measured seismograms and the corresponding dispersion diagrams of the baseline and the repeatline.

APPENDIX B: RAYLEIGH WAVE DISPLACEMENT AND CUMULATIVE ENERGY

For the two-layer model in Table 1, we can calculate the Rayleigh wave velocity and the corresponding displacement vectors for horizontal and vertical components. Fig B1(a) presents the total displacement vector $d(\lambda, z)$ (square root of the horizontal and vertical displacements), as a function of the normalized wavelength (λ/h_1) and depth (z/h_1). Fig B1(b) presents the cumulative amplitude $D(\lambda, z)$, with its definition

$$D(\lambda, z) = \int_0^z d(\lambda, z) dz. \quad (\text{B1})$$

Table A1. Repeatline model parameters and dimensions. h_i : layer thickness; l and w : length and width of model. Scale ratio between the numerical and the experimental model dimensions is 1000.

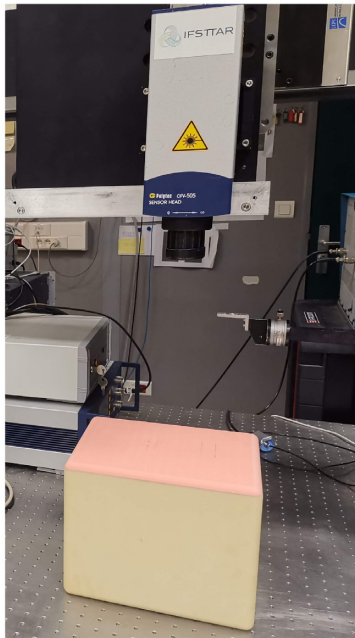
Layer	V_{p_i} (m s ⁻¹)	V_{s_i} (m s ⁻¹)	ρ_i (kg m ⁻³)	ν_i	h_i (mm)	l (mm)	w (mm)
1	1300	703	450	0.29	8.0	265	235
2	2048	1100	1300	0.37	203	265	235



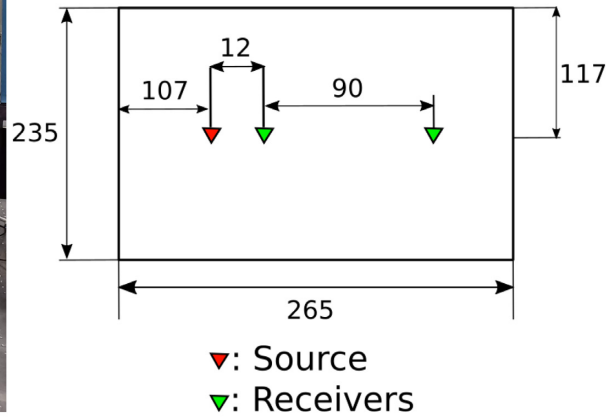
(a)



(b)

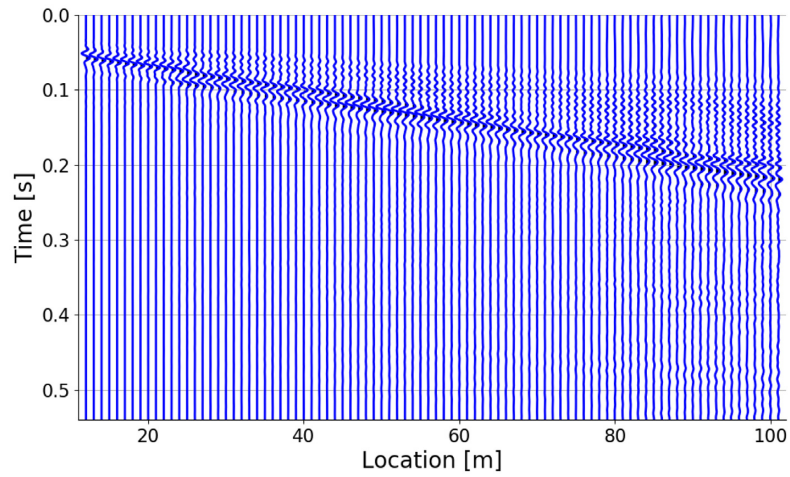


(c)

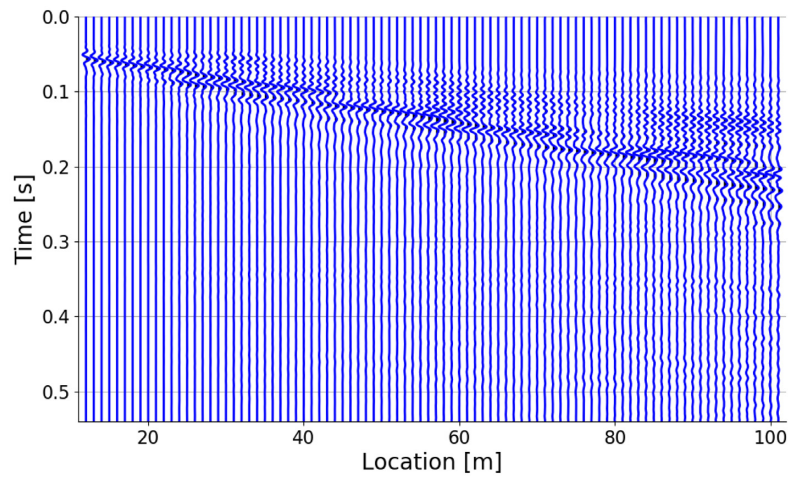


(d)

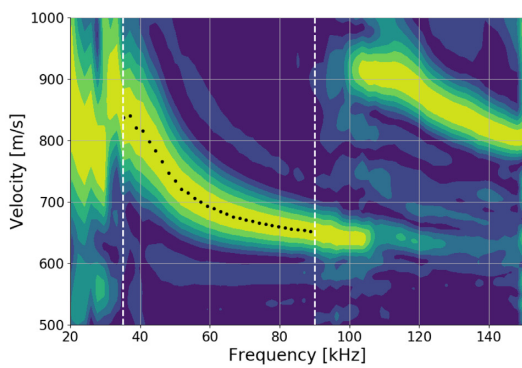
Figure A1. (a) The baseline (left) and repeatline (right) models. (b) The piezoelectric source Acsys®. (c) Experimental set-up and the two-layer resin model. (d) Position of source and the receiver vector.



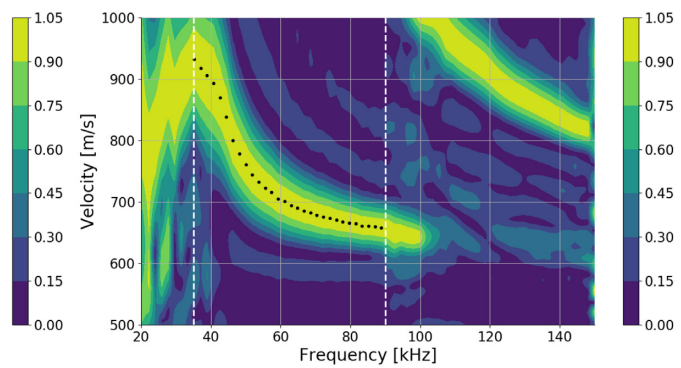
(a)



(b)



(c)



(d)

Figure A2. Measured seismograms of the baseline model (a) and the repeatline model (b), normalized by the maximum amplitude at each trace. Corresponding dispersion diagrams of the baseline model (c) and the repeatline model (d).

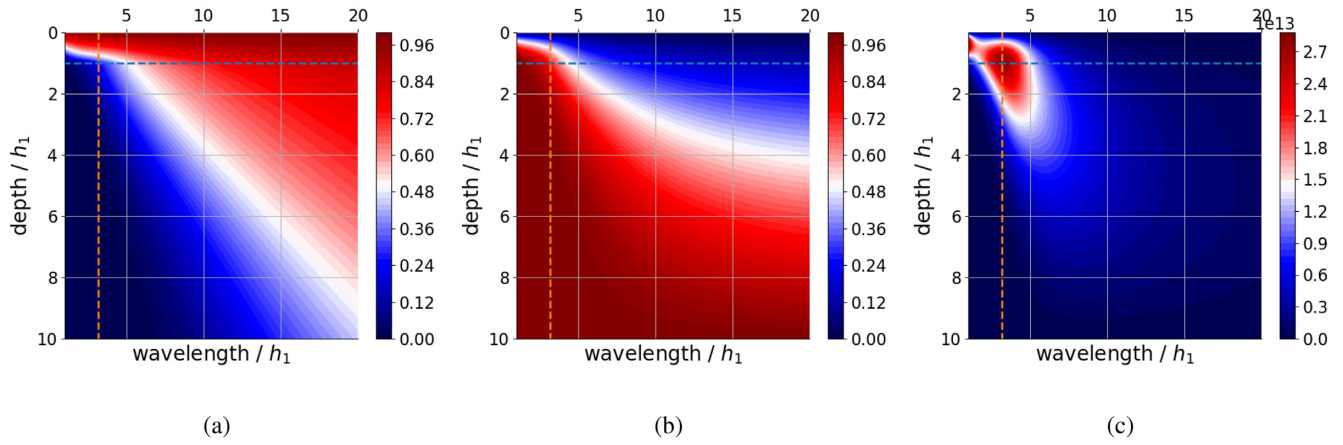


Figure B1. (a) Rayleigh wave displacement vectors as a function of the normalized depth and wavelength. (b) Cumulative amplitude of the Rayleigh wave displacement in the vertical direction (i.e. depth), normalized by the maximum value at each wavelength. (c) Cumulative amplitude derivative with respect to wavelength. The blue line indicates the interface where $\text{depth}/h_1 = 1$. The orange dashed line corresponds to the wavelength $\lambda = 3.2h_1$.